Article:

Staines, KEH and Carrivick, JL (2015) Geomorphological impact and morphodynamic effects on flow conveyance of the 1999 jökulhlaup at sólheimajökull, Iceland. Earth Surface Processes and Landforms, 40 (10). pp. 1401-1416. ISSN 0197-9337

https://doi.org/10.1002/esp.3750

published in Earth Surface Processes and Landforms

Geomorphological impact and morphodynamic effects on flow conveyance of the 1999 jökulhlaup at Sólheimajökull, Iceland

Kate E. H. Staines[1] and Jonathan L. Carrivick[1]

[1]School of Geography, University of Leeds, Woodhouse Lane, Leeds, West Yorkshire, LS2 9JT, UK

Correspondence to:
Dr. Jonathan Carrivick,
Email: j.l.carrivick@leeds.ac.uk
Tel.: 0113 343 3324

Abstract

The 1999 jökulhlaup at Sólheimajökull was the first major flood to be routed through the proglacial system in over 600 years. This study reconstructed the flood using hydrodynamic, sediment transport and morphodynamic numerical modelling informed by field surveys, aerial photograph and digital elevation model analysis. Total modelled sediment transport was 469,800 m^3 (+/- 20 %). Maximum erosion of 8.2 m occurred along the ice margin. Modelled net landscape change was -86,400 m^3 (+/- 40 %) resulting from -275,400 m^3 (+/- 20 %) proglacial erosion and 194,400 m^3 (+/- 20 %) proglacial deposition. Peak erosion rate and peak deposition rate were 650 m^3s^{-1} (+/- 20 %) and 595 m^3s^{-1} (+/- 20 %), respectively, and coincided with peak discharge of water at 1.5 hours after flood initiation. The pattern of bed elevation change during the rising limb suggested widespread activation of the bed, whereas more organisation; perhaps primitive bedform development, occurred during the falling limb. Contrary to simplistic conceptual models, deposition occurred on the rising stage and erosion occurred on the falling limb. Comparison of the morphodynamic results to a hydrodynamic simulation illustrated effects of sediment transport and bed elevation change on flow conveyance. The morphodynamic model advanced flood arrival and peak discharge timings by 100 % and 19 %, respectively. However, peak flow depth and peak flow velocity were not significantly affected. We suggest that morphodynamic processes not only increase flow mass and momentum but that they also introduce a feedback process whereby flood conveyance becomes more efficient via erosion of minor bed protrusions and deposition that infills or subdues minor bed hollows. A major implication of this study is that reconstructions of outburst floods that ignore sediment transport, such as those used in interpretation of long term hydrological record and flood risk assessments, may need considerable refinement.

Keywords: GLOF; outburst flood; glacier flood; erosion; deposition; proglacial;

Introduction

Jökulhlaups (glacier outburst floods) are a sudden outburst of water from a glacial source. These high-magnitude yet relatively infrequent floods can be effective agents of subglacial and proglacial erosion and deposition, causing intense and widespread geomorphological change (Baker, 1996; Björnsson, 2009; Carrivick, 2009). The frequency and potentially the magnitude of jökulhlaups is predicted to increase with climate change and glacier retreat (Pagli and Sigmundsson, 2008; Richardson and Reynolds, 2000; McGuire, 2013; Carrivick and Tweed, 2013) thereby placing more persons and infrastructure at risk from outburst floods. Understanding when, how and why proglacial erosion and deposition occurs during jökulhlaups is therefore crucial for hazard mitigation and landscape management.

The rapid onset of flooding and the short length of time to peak discharge are both characteristics of jökulhlaups and are key reasons why they are poorly understood (Rushmer et al. 2002; Carrivick and Rushmer, 2006; Rushmer, 2007). Direct measurement of flow conditions during jökulhlaups is exceptionally difficult, due to high flow velocities, high flow energy and the sheer volume of water and sediment transported. Furthermore, jökulhlaups tend to occur in remote regions where monitoring and access are limited. Current understanding of jökulhlaup processes and products is therefore largely based on (i) qualitative conceptual models developed from sedimentary studies (e.g. Maizels, 1989a, 1989b, 1991), (ii) geomorphological evidence either from field measurements (Russell et al., 2006) or from remote sensing (e.g. Smith et al., 2006), or (iii) from application of numerical models.

Numerical models applied at the field (landscape) scale to the routing, propagation and proglacial hydraulics of jökulhlaups and other types of outburst flood can be categorised between 1D and 2D types (Table 1). A limitation of 1D models is that hydraulic parameters are calculated based on prescribed channel cross-section positions. In contrast, 2D models can accommodate the complexity of time-transgressive flow typical of outburst floods; flow splitting around islands; transcritical flow, and they can parameterise secondary flow circulation such as is common within major topographical embayments, for example (Carrivick, 2007). However, both 1D and 2D models are capable of accommodating vertical channel changes; i.e. morphodynamics, i.e. erosion and deposition of sediment. Inclusion in numerical modelling of sediment transport and particularly of morphodynamics for real world field-scale outburst floods is very rare but include Carrivick et al., (2011), Worni et al. (2012) and Huang et al. (2014), for example. At the experimental scale, numerical fluid dynamics-based models of sediment transport in outburst floods (e.g. Xia et al., 2010) and morphodynamics (e.g.

Swartenbroekx et al., 2013) are rare and underdeveloped; spatio-temporally variable rheology, bank and bedrock erosion for example have yet to be mechanistically included.

Previous studies on other types of outburst floods unequivocally demonstrate that inclusion of sediment transport and morphodynamics in modelling of the flow is important because: (i) outburst floods often undergo ‘bulking’ and ‘dilution’ due to rapid sediment entrainment and deposition, respectively (e.g. Lube et al., 2012), (ii) entrained sediment affects the mass and momentum energy of a flow (e.g. Fraccarollo and Capart, 2002; Zech et al., 2008; Carrivick, 2010; Carrivick et al., 2011; Iverson et al., 2011; Guan et al. 2014, 2015) (iii) erosion and deposition changes channel geometry, on occasion by over 100 % in a few minutes (e.g. Carrivick et al., 2011), and crucially these three individually and in combination feedback to perturb hydraulics (e.g. Guan et al., 2014, 2015). Furthermore, (iv) sediment transported in a flow can constitute the major hazard associated with outburst floods, impacting structures and burying property, for example.

Flume experiments of outburst floods with mobile sediment (e.g. Capart and Young, 1998; Fraccarollo and Capart, 2002; Pritchard and Hogg, 2002; Cao et al., 2004; Rushmer, 2007; Wu and Wang, 2007; Zech et al., 2008; Emmett and Moodie, 2008; Xia et al., 2010) have emphasised grain-scale erosion and deposition by outburst floods. Whilst several of these experimental studies have informed development of numerical morphodynamic outburst flood models the experiments have been idealised, for example very simple channel geometry, regular-shaped (spherical) particles. Furthermore, with the exception of the work by Guan (2013), they have not been tested at the field scale, which is typically hundreds of metres channel width and many kilometres long. This means that it is unknown whether the grain-scale understanding represented in present theoretical morphodynamic outburst flood models is applicable at the field (landscape) world (Table 1). The only ‘real-world’ applications of fluid sediment transport models to glacial outburst floods, has been that of a multi-phase model; which includes both fluid and granular phases and interactions between them, for the 1994 flood from Lugge Lake in Bhutan by Pitman et al. (2013), and a parallelised 2D hydrodynamic model with coupled sediment transport for the Altai megaflood, by Huang et al. (2014). Overall, numerical computations of (glacial and other) outburst floods are challenging because they must accommodate: (i) highly transient hydraulics, (ii) extreme wetting and drying, (iii) highly irregular topography, and (iv) time-transgressive topography due to erosion and deposition. We note that morphodynamic models have been applied elsewhere in fluvial geomorphology studies.

The aim of this study is to apply a morphodynamic model to a real-world glacial outburst flood or ‘jökulhlaup’, to quantify in unprecedented detail spatiotemporal sediment transport and geomorphological change.

Specifically, we compare 'real' surface changes, as measured by digital elevation models of difference, against numerical morphodynamic model results. Our research question is 'what difference does inclusion of morphodynamics have on outburst flood model output hydraulics, sediment transport and geomorphological work?' Our working hypothesis is that it is crucial to include sediment transport and morphodynamics in field (landscape) scale applications of models for: (i) improved understanding of outburst flood processes and; (ii) for realistic simulations.

Study site

Sólheimajökull is an 8 km long non-surging outlet glacier of Mýrdalsjökull in southern Iceland (Fig. 1). Mýrdalsjökull is located at the south-east end of the 'neovolcanic' zone (Jaenicke et al., 2006) and overlays the Katla central volcano. Of the 16 volcanic systems active in Iceland since 870 AD (Gudmundsson et al., 2008), the Katla system is the second most active and one of the most hazardous (Jónsdottir et al., 2007; Scharrer et al., 2007). Sólheimajökull was selected as the study site for two main reasons. Firstly, this site, like many of the Icelandic glaciers and sandar has been repeatedly photographed since the mid-20th Century. Aerial photographs therefore exist both pre- and post-jökulhlaup, enabling the construction of high-resolution and high-precision digital elevation models (DEMs). Secondly, the proglacial channel system has been exposed to high-magnitude low-frequency glacier outburst floods throughout the Holocene (Maizels, 1991); the 1999 jökulhlaup was the first major flood to route through Sólheimajökull in over 600 years (Russell et al., 2010).

Volcanically-triggered jökulhlaups have occurred at least 17 times since 900 AD (Maizels, 1992; Jónsdottir et al., 2007). The route taken by these jökulhlaups draining from Katla has been determined by the location of the eruption centre, which has migrated over time (Mountney and Russell, 2006; Smith and Dugmore, 2006). Consequently, volcano-glacial jökulhlaups have drained from Mýrdalsjökull along a number of different routes. Eight major jökulhlaups occurred at Sólheimajökull between 4.5 ka BP and the mid-14th Century; after this, the eruption centre of Katla migrated and jökulhlaups were routed through Kötlujökull and across Mýrdalssandur towards the east (Fig. 1). The river flowing from Sólheimajökull, the Jökulsá á Sólheimasandi (abbreviated to 'Jökulsá') flows southwards from the glacier terminus to the North Atlantic Ocean, a distance of ~ 9 km. For most of its length, the Jökulsá is confined to an incised channel that cuts through the extensive outwash deposits of Sólheimasandur and Skógasandur. The sandur deposits are arranged in terraces and fans extending southwards from Mýrdalsjökull.

The 1999 jökulhlaup

The July 1999 was triggered by subglacial volcanic activity within the Katla caldera, which underlies Mýrdalsjökull (Russell et al., 2010) and included drainage of an ice-dammed lake as predicted by Tweed (1998). The 1999 jökulhlaup presents an opportunity for improving understanding of the impact of high-magnitude outburst floods and associated geomorphological impacts in proglacial environments because: (i) inundation extent was directly observed, (ii) peak-discharge estimates were made at the Jökulsá bridge (Sigurðsson et al., 2000; Fig. 1) and (iii) immediate geomorphological impacts were recorded (Russell et al., 2002b; Russell et al., 2000; Russell et al., 2010). These field measurements and observations constrain some of the palaeohydraulic reconstructions presented in this study.

Renewed volcanic activity was apparent in the days prior to the 1999 flood when the water flowing through the Jökulsá á Sólheimasandi changed turbidity (Sigurðsson et al., 2000) and 15 supraglacial cauldrons developed indicating subglacial melting (Russell et al., 2000). Seismic tremors were recorded up to five hours before the release of the jökulhlaup with the peak in seismic activity coinciding with the onset of flooding around 02:00 on the 18th July (Roberts et al., 2003). Water travelled beneath the glacier as a subglacial wave (Russell et al., 2006) and exited from Sólheimajökull at several locations. Four kilometres up-glacier from the glacier terminus, water burst out at the western margin and flowed along the glacier edge where two temporary ice-dammed lakes formed (Russell et al., 2002); one 3.7 km from the terminus and the other in Jökulsárgil (Tweed, 1998). Water also burst through the ice-surface 2 km up-glacier from the terminus, draining supraglacially (Russell et al., 2000). Meltwater exited onto the proglacial zone through a 150 m wide conduit at the western margin of the terminus and also through a conduit at the centre of the terminus. Proglacially, the jökulhlaup was predominantly confined to the main river channel although over-bank flow led to the reactivation of some ice-proximal palaeo-channels (Russell et al., 2002a, b).

The rise to peak discharge was rapid with 1,700 m^3s^{-1} reported by Sigurðsson et al. (2000) as recorded 4 km downstream at the bridge (Figure 1) just one hour after jökulhlaup initiation (Sigurðsson et al., 2000). Peak discharge at the glacier terminus has been estimated at 4,780 m^3s^{-1} from the size of boulders and the velocity required to transport them (Russell et al., 2010) but there must be uncertainty of at least ± 250 m^3s^{-1} on this value due to the range of results from the different methods used by Russell et al. (2010). The jökulhlaup was relatively short-lived; flow levels at the bridge had returned to base-level after approximately 6 hours (Sigurðsson et al., 2000; Roberts et al., 2003).

Present understanding of the geomorphological impact of the 1999 flood can be summarised to be that deposition occurred in supraglacial, ice-marginal and proglacial locations (Russell et al., 2000), with the greatest impact in the ice-proximal zone. A small delta formed in an upper lake basin with sediment depths around 0.1 – 0.5 m thick (Russell et al., 2002a, b). These sediments showed evidence of scouring by ice blocks, indicating strong circulation of shallow flows (Russell, et al., 2002a). In the proglacial area, up to 6 m of sediment were deposited, the source of which was predominantly subglacial excavation (Russell et al., 2000). A 1,200 m^2 boulder fan was deposited in front of the western side of the glacier terminus with boulders > 10 m in diameter (Russell et al., 2010).

Methods

Each palaeohydraulic modelling technique has its own assumptions and limitations, so several were used in this study in combination with field-based surveys, aerial photograph analysis and terrain analysis to reconstruct sediment transport and geomorphological impact.

Palaeocompetence measurements

Clast measurements focussing on the largest clasts only were made at the ice-proximal boulder fan for the purpose of reconstructing flow velocity using the palaeocompetence method. This method is based on relationships between incipient clast motion, clast entrainment and flow velocity (Costa, 1983). However, whilst such techniques enable estimates to be made on flow velocity, shear strength and viscosity (Maizels, 1989b), they are based on flume experiments with gravel < 35 mm, assume an unlimited sediment supply (calibre and volume), are assumed to pertain to peak discharge, and are restricted to at-a-point in space, so must be used with extreme caution (e.g. Carrivick et al., 2013b). With these limitations and assumptions in mind, the palaeocompetence method was used in this study only to give independent comparison with the hydrodynamic and morphodynamic modelling. The a, b and c axes lengths of 395 boulder clasts were measured on the ice-proximal boulder fan; these clasts were selected subjectively but with an aim to cover the whole fan area and to preferentially sample the largest clasts to provide a minimum estimate of spatially-distributed flow competence. The length of the intermediate axis of each boulder clast was used to reconstruct flow velocity (v), shear stress (τ) and stream power (ω) using the equations of Costa (1983). The channel slope near the boulder fan was 0.0275 m/m (Russell et al., 2010). Proglacial hydraulic roughness was estimated at Manning's n = 0.05 during field surveys and this agrees with that in Fig. 9 of Russell et al. (2010). To maintain consistency and to permit inter-model comparisons, the same value of Manning's n was used for palaeocompetence reconstructions and for hydrodynamic and morphodynamic modelling.

Morphodynamic modelling

Morphodynamic modelling was used to reconstruct spatiotemporal flow hydraulics, sediment transport and geomorphological impact and specifically utilised depth-averaged modelling within (the now open source) Delft3D (Delft Hydraulics) model software. This model is a multi-dimensional hydrodynamic and morphodynamic simulation programme that is numerically stable for unsteady flow conditions. It solves the Navier–Stokes equations for an incompressible fluid under the shallow water and the Boussinesq assumptions. The former of these assumptions reduces the vertical momentum equation to a hydrostatic pressure equation and the latter assumes that momentum transfer caused by turbulent eddies can be represented with a user-specified eddy viscosity value. The key model equations are given elsewhere; by Lesser et al. (2004) and by Carrivick et al. (2009) for example but here it is important to note that this is a fluid model not a multi-phase model. Furthermore, there is no bank erosion in terms of 'mass failure', only grain by grain entrainment and deposition. Depth-averaged simulations were preferred over 3D modelling because horizontal flow conditions were expected to predominate over vertical motion and were of greater interest in this study.

<u>Computational domain and mesh formation</u>

Model equations were formulated on an orthogonal curvilinear mesh, which was defined in spatial extent, shape and spatial resolution by the same properties of terrain elevation points extracted from panchromatic black-and-white stereo-pair aerial photographs in digital format (having been photogrammetrically scanned at 15 microns or 1800 dpi) with a ground pixel size of < 1 m. Pre-flood aerial photographs were taken in August 1996 and post-flood aerial photographs date from August 2001. Both sets were sourced from Landmaelingar Islands (LMI) and orthorectified in Leica Photogrammetry Suite (LPS) with ground control points (GCPs) generated using a Leica GPS500 dual phase differential Global Positioning System (dGPS). Although it is acknowledged that some parts of the landscape could have changed slightly in the 3 years between the pre-flood aerial photograph survey and the 1999 jökulhlaup it was considered preferable to use a pre-flood terrain model rather than a post-flood landscape, as is often the case in jökulhlaup reconstructions. Indeed, other studies should note that quantifying sediment transport and geomorphological impact of jökulhlaups and of other outburst floods will be very difficult if only a post-flood landscape terrain model is available.

The pre- and post-flood Digital Elevation Models (DEMs) had regular grid cells of size ~ 2m. DEM errors and uncertainty was assessed by comparing grid cell values to dGPS-derived spot elevations and to a DEM constructed from a summer 2010 airborne LiDAR survey, which for our purposes we assumed had no error. Uncertainty in our photogrammetrically-derived 1996 and 2001 DEMs was assessed by automatically defining 400 random points sampled across each DEM, the dGPS and the LiDAR datasets and only in areas suspected not to have changed in elevation; i.e. excluding the glacier and the proglacial braidplain. Comparisons of the elevations of these 400 points revealed a heterogeneous error, and were used with inverse distance weighting interpolation to generate an error surface, which was then used to correct the two DEMs (Staines et al., 2014). Errors were greatest in steeper and more rugged areas, as expected (e.g. Hopkinson, Hayashi and Peddle 2009; Huggel et al. 2002), although we think that a proportion of these 'errors' could indeed have been real landscape change in the form of hillslope activity. Final 1996 DEM error was quantified with mean elevation difference of -0.03 m and RMSE of 0.89 m, and final 2001 DEM error was quantified with mean elevation difference of 0.002 m and RMSE of 1.24 m (Staines et al., 2014). Assessment of uncertainty in our volume calculations follows the method of Lane et al. (2003) whereby we use 'unthresholded' DEMs of difference, because differences below the level of detection are uncertain, and where volumetric uncertainty, σ volume, as considered when producing DEMs of difference (DoDs) is calculated as follows:

$$\sigma\ \text{volume} = d^2\sqrt{n}\ \sigma DoD$$

where d is raster cell size, n is number of raster cells for which the DEM of difference is calculated, and σDoD is the error of the DEM of difference as given by $\sqrt{\sigma\_DEM\#1^2 + \sigma\_DEM\#2^2}$, where σ is the standard deviation of residuals. This method indicates that when we differenced the 1996 and 2001 DEMs uncertainty in our elevation values was 1.53 m and in our volume changes was 0.009 km^3 (Staines et al. 2014). However, we consider these uncertainty values to be a 'worst case scenario' because: (i) the quality of photogrammetry-derived DEMs is best in areas of low relief and high-contrast, such as proglacial areas, and; (ii) as Staines et al. (2014) show in their Table 2 whilst absolute elevation error in the proglacial area cannot be assessed, because it cannot be certain that those points are static, volumetric uncertainty over the valley floor is approximately half that of the DEM in its entirety.

Spikes and sinks were removed and the terrain 'inverted' in ArcGIS to produce a bathymetric xyz file (i.e. positive elevations beneath 0 m) for the model. The x and y coordinates in this file demarked an extent and shape around which user-specified splines crudely defined the mesh shape (Fig. 2) and were then refined automatically to give an orthogonal curvilinear mesh (Fig. 2) with each mesh cell resolution ~ 2 m in the lateral direction and ~ 10 m (at most ~ 15 m) in the longitudinal direction. To reduce file sizes and hence computation times, the mesh was clipped to the extent of the main river channel (Fig. 2), as observations during the jökulhlaup established that flow was confined to this channel (Sigurðsson et al., 2000). The bathymetry xyz points were mapped onto the mesh (Fig. 2) using the Delft3D QUICKIN module using grid-cell averaging.

Input data to numerical model

The model proglacial channel was 'pre-wetted' by running base flow (without sediment transport or morphological updating) up to 90 $m^3 s^{-1}$ which is the bankfull discharge under 'normal' flow conditions at the bridge (Lawler, 1994; Lawler and Brown, 1992). Hydraulic conditions at the last time-step of the baseflow model were used as the input ('restart') file for the jökulhlaup model.

Water discharge was introduced to the jökulhlaup model at both the western side of the glacier terminus and at the terminus centre. These positions were chosen on the basis of field observations of the main glacial drainage conduits at the time of the flood (Russell et al., 2002b; Russell et al., 2000; Russell et al., 2010). Field observations (Matthew Roberts, pers. comm.; Russell et al., 2010) indicated that the western conduit was the main drainage channel both before and during the 1999 jökulhlaup and therefore we defined 40 % of the total discharge exited from at the central conduit and 60 % from the western conduit (Fig. 3). The jökulhlaup model initial hydrograph (Fig. 3) was best-fit to the magnitude (1,700 m^3s^{-1}) and timing (one hour after initiation) of peak discharge, and flood volume, as recorded 4 km downstream at the bridge (Sigurðsson et al., 2000; Roberts et al., 2003). In more detail, the jökulhlaup model input hydrograph peak discharge, duration and shape (Fig. 3) was based on: measurements of river stage and discharge of 1700 $m^3 s^{-1}$ made at the bridge by Sigurðsson et al. (2000); the peak discharge estimates of Russell et al. (2010) and; knowledge of the flood trigger. Russell et al. (2010) suggested that downstream flow attenuation was considerable but we regard that the input discharge of 4,000 m^3s^{-1} as reconstructed by Russell et al. (2010) is rather high for our usage because we had to run the model with no sediment input at the discharge point. Russell et al.'s (2010) boulder fan evidences that boulder-sized clasts were moved, implying rapid deposition because very few boulders occur farther downstream. However, neither the total volume nor the temporal flux of this subglacially-derived sediment transport is known and cannot even be reasonably estimated. Therefore, our jökulhlaup model was necessarily run with no subglacially-derived sediment. Thus to be clear, our modelled flow was initially 100 % water because any sediment in the model is that from the proglacial area only.

The model time-step was set at 0.005 minutes to accommodate rapidly varying hydraulics and rapidly varying channel bathymetry. Horizontal eddy viscosity was defined at 0.01 m^2s^{-1} and the horizontal eddy diffusivity at 10 m^2s^{-1}; both of these parameters affect advection of mass and momentum and concern momentum transfer caused by turbulent eddies but scale depending on mesh cell size. Whilst there is little advice on setting eddy viscosity and eddy diffusivity values, over a braided gravel bed river reach Williams et al. (2013) found that an eddy viscosity of 0.01 m^2s^{-1} produced model errors in terms of depth and velocity that agreed well with independently-measured field data.

Model sensitivity was assessed against peak discharge magnitude and timing (at the bridge), which are the only measured and thus relatively certain properties of the 1999 jökulhlaup. However, modelled peak discharge magnitude and timing was sensitive to roughness, which we defined with Manning's n (Fig. 4). Figure 4, which illustrates a cross-section near the downstream model boundary, demonstrates that varying Manning's n does not produce a linear response in discharge, and this is because of the morphodynamic part of the model and feedbacks between sediment entrainment and flow hydraulics, as partly suggested by the response of bed elevation change to varying Manning's n (Fig. 4). Therefore, bed roughness was defined as a uniform value of 0.05 across the whole mesh, with respect to the channel substrate that we have observed in the field and as has been reported by Russell et al. (2010). We note that Manning's n values used for other proglacial areas comprising sand to cobble sized materials has varied from 0.04 to 0.06 (Alho and Aaltonen, 2008). For interest, the model was not sensitive to other user-specified parameters including mesh resolution and grain size distribution, in agreement with the findings of model (in)sensitivity by Guan, (2013) and Huang et al. (2014).

For the purposes of modelling sediment transport, three sediment fractions were defined on the basis of the sedimentological observations reported by Russell et al. (2010) and our own sedimentological analysis (Staines et al. 2014). These sediment fractions were: boulders (D_{50} = 400 mm); cobbles (D_{50} = 100 mm) and; granules (D_{50} = 3 mm), all with specific density of 2680 $kg.m^{-3}$, which is typical for the basalt-dominated geology. Non-cohesive suspended sediment transport was computed by solving the 3D advection–diffusion (mass-balance) equation and by imposing a reference concentration at a reference height following the method of van Rijn (1993). Bedload was computed in two stages: (i) calculating transport magnitude and direction at mesh cell centres using the Meyer-Peter-Müller (1948) 'MPM' equation for bedload, and; (ii) computing bedload transport rates at cell interfaces. We note that the MPM formulae was developed via flume experiments and thus its applicability for the range of sediment sizes observed in the field is questionable, but there is no alternative equation suitable for coarse sediment transport. The MPM formulae was implemented in Delft3d using the mean grain size from the fraction being considered. An option in Delft3d for considering ‘hiding and exposure’ effects by adjusting the effective critical shear stress for fine-grained sediments whilst lowering it for coarse sediments was not used in this study because of the lack of information on a suitable multiplicative factor to use.

Suspended sediment transport included consideration of suspended sediment on fluid density, settling velocity, interaction of bed sediment fractions and inclusion of a fixed layer. In overview, the transport of suspended sediment was calculated by solving the three-dimensional advection-diffusion (mass-balance) equation for the suspended sediment. Density effects of suspended sediment fractions in the fluid mixture were recognised by adding (per unit volume) the mass of all sediment fractions, and by subtracting the mass of displaced water. The settling velocity of the (non-cohesive) sediment fractions were computed depending on the diameter of the sediment in suspension. Sediment transfer between the bed and the flow was modelled using sink and source terms acting on the near-bottom layer. The mathematical form of these sediment transport calculations are given by Carrivick et al. (2010) and so are not repeated here for brevity.

An initial bed thickness of 5 m was defined for each sediment fraction, set as uniform across the computational mesh, and based on (i) representative GPR surveys in the vicinity of the river channel of sediment thickness and (ii) sediment exposures in river banks (Staines et al., 2014). Note that there was no consideration in the model of the stratigraphy of these sediments; all fractions were available in all three layers and all grains were available for entrainment simultaneously. The total of 15 m sediment depth was not exhausted by the model, which seems sensible given that there are no bedrock sections of the river. The downstream boundary of the model at the Jökulsá estuary is tidal (Mountney and Russell, 2006) and so was defined as ‘open’ with ‘uniform water level’ set as 0 m.asl. Downstream boundary tide water level changes were assumed to be negligible due to the short time-frame of modelling.

Morphodynamics were modelled by considering that if there was sediment deposition of y (m) within a grid cell of z m.asl. at timestep ‘x’, then that grid cell was updated accordingly to give a sediment thickness of z + y (m). Sediment erosion was modelled correspondingly, to cause a reduction in sediment thickness. Updated sediment thickness then informed updated bathymetry and this bed elevation then perturbed flow hydraulics at time step x+1. There was no inclusion of stratigraphy, i.e. no calculation of the order in which sediments were deposited, and thereby we assume that vertical sorting was not a major control on rates or volumes of deposition. Erosion and deposition volumes were computed from the difference in elevation grids output at 10 min intervals.

Quantifying uncertainty in our model calculations is difficult because it is due to a combination of factors. For the hydrodynamic model, the factors affecting model uncertainty are the: input 1996 DEM (± 0.03 m); input hydrograph (± 250 m^3s^{-1}); specified roughness (field-measured), and; hydrodynamic model formulations. For the morphodynamic model, and in addition to the factors mentioned for the hydrodynamic model, the factors affecting model uncertainty are the: sediment grain size distribution (field-measured), and; sediment transport model formulations. Since the hydrodynamic model was best-fit to the peak discharge timing and flood volume as recorded at the bridge, 4 km downstream, model uncertainty cannot be constrained from a comparison of modelled versus measured hydrographs. Morphodynamic model uncertainty cannot be constrained from a comparison of the simulated and observed net change in sediment storage because as will be discussed there are different time scales involved in these two calculations. Therefore both hydrodynamic and morphodynamic model uncertainty estimates must recognise that: (i) there are components of the model that cannot be quantified for uncertainty; (ii) that these uncertainties propagate through the model work flow and act in combination, and (iii) that there are some facets of model behaviour that might not be so well simulated. Overall, given the factors in the model for which we can quantify uncertainty, given our field knowledge and measurements, and given our previous experience of applying the model to outburst floods (e.g. Carrivick, 2006, 2007; Carrivick et al., 2009, 2010, 2013a) we estimate uncertainty in hydrodynamics to be within +/- 10 %, uncertainty in erosion and deposition (morphodynamics) to be within +/- 20 %, and summative/net landscape change to be within +/- 40 %.

Results

Palaeocompetence reconstructions

The ice-proximal boulder fan clasts have a bimodal size distribution, with the greatest frequency of clasts measured in the ‘small cobble’ and ‘large boulder’ categories (Fig. 5). Palaeocompetence reconstructions, using just the 5 largest boulders to suggest maximum values, suggest that peak flow velocity was ~13 $m.s^{-1}$ and peak flow depth was 7.6 m (Table 2). Boulder size decreased rapidly downstream (Fig. 6A) and therefore flow parameters were also calculated for each individual boulder (clasts > 256 mm in diameter) and visualised in ArcGIS (Fig. 6B). Flow velocity ranged from 14 $m.s^{-1}$ at the ice proximal end of the fan to 2.4 $m.s^{-1}$ at the ice-distal end. Stream power varied from approximately 75 to 35,400 $W.m^{-2}$ and boundary shear stress from 36 to 3,000 $N.m^{-2}$. Flow depths varied from just under 10 m ice-proximally to 0.6 m at the ice-distal end of the fan. A comparison of the palaeocompetence reconstructions with the slope area and numerical modelling methods are given in Table 3.

Morphodynamic modelling

This study ran morphodynamic models lasting ~ 24 hours in computational time on a desktop PC with a 3 Ghz processor, 8 Gb RAM and a 1 Tb hard disk.

Flood inundation

Flow was largely constrained within the post-LIA incised Jökulsá channel, although some palaeo-channels were re-activated (Fig. 7). The dominant area of channel reactivation was approximately 500 m south of the glacier, where flow was routed through palaeo-channels on the older moraine surface (Fig. 7). These channels were located 2 to 3 m above the pre-jökulhlaup active river channel. Beyond this point, modelled flow was confined to the steeply-incised channel for 1 km between the moraine. At the downstream opening of this confinement, the older (dry) sandur surface was reactivated between this point and the Jökulsá road bridge (Fig. 7). Simulated flow built up behind the Jökulsá road-bridge embankment, approximately 5 km downstream, eventually flowing over the road south of the Jökulsá bridge at 60 minutes We do not know if this happened in reality, but as outlined in the methods section, the road bridge had been removed from the pre-flood DEM, leaving a 160 m wide opening between the road embankments on either side of the river. Previously dry, vegetated channels were inundated along much of the channel (circled area on Fig. 6). By the end of the simulated jökulhlaup, these channels were dry. At the Jökulsá estuary, flow ponded behind the low-relief sand-dune ridge to the west of the river (Fig. 7).

Spatiotemporal variations in modelled hydraulics

The overall spatial pattern of modelled flow depth and flow velocity are mapped in Figure 8 at time 01:30 after flood initiation, i.e. near peak flow conditions. The pattern distinguishes channelled flow, overbank flow and braided flow (Fig. 7). In detail, the pattern of flow velocity and flow depth is ‘smoother’ or more spatially coherent, in the morphodynamic simulation compared to the hydrodynamic simulation. Bed elevation changed as a result of erosion and deposition and showed considerable variability along the channel. In ice-proximal zone progressive erosion occurred, in channelized areas (cross-section 3) rising stage erosion occurred and falling stage deposition, in distal reaches rising stage deposition and falling stage erosion occurred (Fig. 8). Figure 8 also plots the temporal model output of flow velocity, water depth and bed elevation change at selected points on each of the cross-sections. These temporal comparisons between the hydrodynamic and morphodynamic model output illustrate the effects of including sediment transport and iterative (per model time step) bed elevation change on flow conveyance and are summarised in Table 4, namely: no effect on total inundation area; nearly double frontal wave speed; timing of peak stage advanced by about 19 %; no significant effect on peak flow depths or peak flow velocities; a strong effect on the rate of change of flow depth and flow velocity.

The detail of the morphodynamic simulation was further examined at seven cross-sections as indicated in the last panel of Figure 7 and were chosen in location to permit (i) analysis of the longitudinal evolution of the flood, (ii) comparisons with those considered by Russell et al. (2010) and (ii) comparison against the bridge record of Sigurðsson et al. (2000). Spatiotemporal quantification of depth-averaged velocity, average bed shear stress, total sediment transport (sum of all fractions) and flow discharge are provided as suppl. material video and for brevity and ease of reporting in this paper were recorded at each cross-section (Fig. 9). Flow discharge exhibited a steep rise to peak values and a shallower falling limb. Peak discharge at cross-section 1 was reached after 30 minutes and after 60 minutes at each other cross-section (which is not surprising because the input hydrograph was best-fitted to the peak discharge magnitude and flood volume at the bridge). The magnitude of peak discharge ranged from 1,600 m^3s^{-1} at cross-section 1, to 2,500 m^3 s^{-1} at cross-section 3, and 2,000 m^3 s^{-1} at cross-section 6 (Fig. 9).

Depth-averaged velocity at peak discharge (one hour after flood initiation) was highest at the glacier terminus, reaching 12 $m.s^{-1}$ at the northern conduit (Fig. 9). Flow velocity decreased rapidly to ~ 4 m s^{-1} in the immediate proglacial channel, but increased in the constricted section of the channel cut through moraine (Fig. 9). Cross-sectional averaged velocities showed a similar downstream pattern to discharge, with average velocities lower in cross-section 1 (Fig. 9). The time at which peak velocity was reached varied with distance downstream. Peak flow velocity was reached after 30 minutes at cross-section 1 and after 60 minutes at cross-sections 2 to 5 (Fig. 9). At cross-sections 6 and 7, velocity remained near constant between 60 and 90 minutes Bed shear stress ranged from 60 to 580 $N.m^{-2}$ at peak discharge, 30 minutes after flood initiation. Bed shear stress was highest where velocities were highest except at cross-section 2, where bed shear stress was greatest at 180 minutes after flood initiation (Fig. 9).

<u>Patterns, volumes and rates of geomorphological change</u>

The modelled volume of total sediment transport (the sum of the three sediment fractions) was 469,800 m^3 (± 20%) (Table 4). The rate of modelled total sediment transport at cross-section 1 peaked at 0.25 $m^3s^{-1}m^{-1}$ 30 minutes after flood initiation (Fig. 9). With progression of time, modelled total sediment transport became more 'flashy', that is, the peak of curve was steeper. This is in contrast to modelled discharge, which became less flashy through time and with distance downstream (Fig. 9). Total sediment transport generally decreased with distance downstream (Fig. 9). Maximum erosion of 8.2 m occurred along the ice margin (Fig. 10) and 5.9 m of erosion occurred at 2.4 km down valley. This latter site was also the site of maximum deposition at up to 3.2 m.

The total change in the differenced DEMs = -415,200 m^3 (± 9,000 m^3) which is ~ 55,000 m^3 less than suggested by the morphodynamic model. This difference in volume between what we have modelled and what we have measured could be an indication of: (i) the amount of subglacially-sourced material; (ii) geomorphological activity that has occurred during the flood; i.e. incision and infill, (iii) geomorphological activity between the flood and the DEM survey dates; (iv) a reflection of measurement error. The modelled landscape change was compared on a grid cell by grid cell basis to the DEM of difference (DoD) and whilst visually the agreement is generally good spatially (Figure 11A), and to a lesser extent along a long profile (Figure 11B), there was no statistical correlation for either. Four zones highlighted by white circles in Figure 11A indicate discrepancy between the the DoDs, as highlighted in the 3rd panel difference measured minus modelled map. These differences in the white ellipse zones suggest: (i) incision of bar forms probably after the 1999 flood but before the re-survey in 2001, and; (ii) lateral bank (mass collapse) erosion, which is not accounted for in the morphodynamic model. The ice-marginal difference (red zone) in the difference map is the boulder fan; demonstrating the subglacial provenance of this material during the 1999 flood and the ignorance of this in the morphodynamic model. The long profile depicted in Figure 11B could be interpreted to indicate under-prediction of erosion and deposition by the model, but with consideration of the results of Staines et al. (2014) may actually just reflect subsequent landscape response to the jökulhlaup (between the flood date and the 2001 aerial photograph survey) as over-steepened unconsolidated banks collapsed and ablation-fed meltwater incised jökulhlaup deposits, for example.

The net landscape change during the modelled jökulhlaup as measured by the total modelled elevation change was -86,400 m^3 (± 40%), resulting from -275,400 m^3 (± 20%) proglacial erosion and 194,400 m^3 (± 20%) proglacial deposition. These quantities are interesting because they are measures of geomorphological work and will permit comparison to other geomorphological processes that mobilise a relatively large volume moved over a relatively short time period. The modelled net loss of -86,400 m^3 (± 40%) indicates the volume of sediment that was transported into the sea in just 7 hours. Total erosion and deposition per grid cell and were discriminated for both the rising and falling limbs of the modelled jökulhlaup (Fig. 12). The pattern of elevation change was ‘smoother’ or most ‘spatially coherent’ during the falling limb (Fig. 12). The rising limb pattern suggests widespread activation of the bed, whereas the falling limb pattern suggests more organisation, perhaps pseudo bedforms. In ice-proximal positions, the morphodynamic model produced substantial channel incision with a 10 m vertical decrease in bed level measured at cross-section 1 (Fig. 10). Just north of the Jökulsá bridge at cross-section 4, deposition was observed to the west of the main channel, which corresponds well with post-jökulhlaup observations made in the field (Russell et al., 2010). In ice-distal positions at cross-section 7, large-scale bars and channels formed: two main channels formed at 350 m and 420 m along the cross-section transect and deposition occurred at the channel margins (Fig. 10).

Both peak erosion rate and peak deposition rate coincided with peak discharge and were 650 m^{3}s^{-1} and 595 m^{3}s^{-1}, respectively. Qualitatively, erosion proceeded rapidly as a result of intense bed shear stress on the rising stage of the flood (Fig. 9; suppl. material video). However, there was some re-deposition on the rising stage of the flood (suppl. material video). Peak erosion rate was ~ 650 m^{3}s^{-1} and the peak deposition rate was ~ 580 m^{3}s^{-1}, both occurring at the peak stage at 1.5 hours after flood initiation. During the falling limb, bed shear stress diminished and we also note that the total erosion volume and deposition volume did not significantly change. However, there was some waning stage incision of sediments as evidenced by the decline in bed elevation in the later part of the event (Fig. 8). We note that more sophisticated analyses of the patterns of erosion and sedimentation should consider the spatial stress divergences/convergences as the fundamental control on channel morphological response, but we have not done that here because of the lack of a statistical correlation between our modelled elevation changes and measured elevation changes.

Discussion

Comparison of reconstruction methods

Palaeocompetence calculations were performed to provide an independent comparison to the numerical modelling, but there is a big discrepancy in the hydraulic reconstructions by the palaeocompetence and numerical modelling methods. Palaeocompetence-derived hydraulic values are higher than those obtained from the numerical modelling (Table 3) but only pertain to the boulder fan whereas the numerical modelling included the entire proglacial channel (Fig. 8). For example, maximum flow depths reconstructed by each method ranged from 4.8 m using the slope-area technique (Russell et al., 2010) to 9.7 m using the palaeocompetence method (Table 2) to 12 m using distributed numerical modelling. We interpret the discrepancy in reconstructed hydraulics to highlight the assumptions (and thus limitations) inherent within each method. Firstly, palaeocompetence techniques rely on ‘scaled-up’ relationships between gravel-sized clasts and hydraulic parameters and therefore erroneous results are likely for large boulders (Cook, 1987; Jarrett, 1987). Indeed Costa (1983) stated that palaeocompetence reconstructions for clast greater than 2 m in diameter are less reliable than those generated from smaller clasts. Secondly, the palaeocompetence technique assumed that sediment supply to a flood was unlimited (Carrivick 2007, 2009) and therefore provides a minimum estimate of flow parameters. It is possible that clasts larger than those measured could have been transported if they were available. Thirdly, in highly turbulent floods, lifting forces can encourage the entrainment of clasts larger than those transported by flow-velocity and tractive forces alone (Costa, 1983).

Regarding the discrepancy between Russell et al.'s (2010) slope area results and our morphodynamic modelling, Russell et al.'s slope area reconstructions were applied only at discrete cross-sections and necessarily assumed gradually-varied flow conditions. They estimated flow velocity in part via grain roughness; i.e. boulder measurements, so with the same limitations as outlined for the palaeocompetence methods above. Perhaps most crucially, they were applied on the post-flood terrain. In contrast, our morphodynamic modelling input a pre-flood DEM, specified an input hydrograph and pre-existing sediment across the model domain, and modelled fully spatiotemporal hydraulics, sediment transport and subsequent geomorphological change.

Comparing the hydrodynamic model with the morphodynamic model, inclusion of sediment transport and morphological updating did not affect the total inundation area. However, it did cause the frontal wave speed to nearly double (Table 4). This is due to loss of energy in sediment entrainment and flow resistance and at the leading wave front edge, c.f. experiments by Carrivick et al. (2011). It suggests that usage of numerical models of outburst floods in a hazard analysis should include morphodynamics if the time to inundation is important. The same suggestion can be made again because the timing of peak stage was advanced by about 19 % by including morphodynamics (Table 4). Generally, morphodynamics did not alter absolute values of peak flow depths or peak flow velocities very much, in general agreement with the findings of Huang et al. (2014), but did affect the rate of rise and fall of these parameters (Figs. 7 and 8). Attributing these differences to sediment transport and morphodynamic processes demands more work to (i) define the spatiotemporal mass and momentum of the fluid, and (ii) examine spatiotemporal channel geometry changes in greater detail, for example vertical versus lateral changes and the relationship (feedback?) between changing channel cross-section and hydraulics.

Proglacial jökulhlaup character and impact

A key advantage of morphodynamic over hydrodynamic modelling that it provides quantification of erosion and deposition patterns, volumes and rates that would otherwise be unobtainable. Whilst parameterising a morphodynamic model requires good knowledge of the flood event and of the flood channel before the event, that effort is rewarded with improved process and product understanding. Whilst it must be remembered that there are errors in the DEMs (Staines et al., 2014) and assumptions in the morphodynamic modelling, the main differences between the two (Fig. 12) are likely to be due to the different time-scales considered: 5 years between the DEMs versus a few hours for the model. That said, the remarkable similarity in pattern (Fig. 11) gives confidence in both the DEMs and the model and demonstrates that the 1999 jökulhlaup had an important geomorphological impact on the proglacial area.

Overall, erosion and deposition both occurred in the main channel, and both were greater in narrower reaches (Fig. 11). Erosion was greater in narrower reaches because the water depth was deepened and velocity was higher, which induced more sediment movement. The erosion maps, and the more coherent flow structures in the morphodynamic model (Fig. 8), together suggest that morphodynamic processes make flow conveyance more efficient via smoothing of the bed and straightening of the channel sides in combination subduing form roughness. We suggest that deposition was greater in narrower reaches because the (finite) amount of sediment being transported was redistributed over a relatively small area, in comparison to wider reaches. The slight increase in peak discharge observed at cross-section 2 (Fig. 9) is likely a response to changing channel geometry because flow was constricted to a single channel between the moraine belt 2 km downstream of the glacier terminus. Beyond this constriction the flood routeway becomes wider with increased distance from the glacier and shallower in gradient. Correspondingly net deposition was observed as a result of reduced velocities and reduced bed shear stress, which is similar to expansion fans and valley-fill sediment documented by Alho et al., (2005), for example.

The evidence in the morphodynamic model results of rising-stage deposition and waning stage incision has considerable promise for quantitatively assessing the conceptual models that have been developed from sedimentary (e.g. Maizels, 1989a, 1989b, 1991) and geomorphological observations and measurements (Russell et al., 2006). During the rising limb of the jökulhlaup ice-proximal deposition was modelled at the glacier terminus (Fig. 11). This is interesting because ice-proximal deposition was observed during the jökulhlaup, the boulder fan being the key depositional impact of the flood (Russell et al, 2010). Falling stage coherence of elevation changes (Fig. 11) is potentially indicative of bedform development (c.f. Rushmer 2007). Volcano-glacial jökulhlaups frequently exhibit a rapid rising stage, during which proximal aggradation rates are high and downstream transport is limited (Rushmer, 2007).

A note on the post-jökulhlaup landscape response

The post-jökulhlaup period at Sólheimajökull has been characterised by glacier retreat (Staines et al, 2014). Sólheimajökull retreated on average 40 m yr^{-1} between 1996 and 2010. Owing to a subglacial overdeepening, channel incision occurred ice-proximally, leading to the abandonment of the boulder fan altitudinally above the present-day channel. As a result, the boulder fan has only been subject to minor re-working post-jökulhlaup. Landscape change in the lower channel reaches in the decade following the jökulhlaup was characterised by net channel aggradation. Between 2001 and 2010 there was a progressive increase in downstream channel braiding, suggesting that sediment deposited by the jökulhlaup is moving through the proglacial channel system, being re-distributed by non-jökulhlaup flow.

A note on modelling approaches

Outburst flood modelling inevitably involves a series of uncertainties associated with the difficulties in estimating the values of key parameters. Notwithstanding the excellent pre- and post-flood data we have used in this study, it has been necessary to consider uncertainty propagation through the investigation. We could not define sediment input from a subglacial source and whilst we could have an insight to the volume of this subglacial sediment (as the difference between our model and the DoD), the subglacial sediment flux remains unknown. Considering subglacially-sourced sediment will of course not be a problem for studies of glacial outburst floods from ice-marginal lakes. For studies of any sort of outburst flood, it could be considered that studies who have very limited field data could find that the parameterisation of roughness could be as important as the model structure employed. Indeed the wider challenge of how to use limited observational data to support high-resolution predictions is certainly unresolved. In contrast to the mechanistic approach, such as the 'natural test case' of this study, an alternative approach is to acknowledge that actually none of the model inputs are known, except within reasonable bounds, and then to conduct Monte Carlo scenario-based modelling where each variable and combination of variables is systematically varied to define 'most likely' outputs.

Conclusions

The key contribution of this study is a demonstration that the morphological adjustments induced by the passage of a glacial outburst flood (GLOF), or 'jökulhlaup', are significant enough to significantly and dynamically affect the conveyance characteristics of the flow. A major potential implication of this work, therefore, is that if reconstructions of outburst flood hydraulics for interpretation of the long term hydrological record and flood risk assessment could be with significant error. Assessment of differences in flow velocity and flow depth simulated in cases where the model had either a fixed bed or a moveable bed was opportunistically employed for the 1999 Sólheimajökull jökulhlaup, which acted as a 'natural laboratory', because modelled sediment transport and geomorphological change was able to be compared to the difference between pre- and post-flood topography as measured using photogrammetrically-derived DEMs.

Firstly, this analysis has revealed new insights into the proglacial character and behaviour of the 1999 jökulhlaup event. Total sediment transport was 469,800 m^3 (± 20 %) (Table 4). Maximum erosion of 8.2 m occurred along the ice margin (Fig. 10) and 5.9 m of erosion occurred at 2.4 km down valley. This latter site was also the site of maximum deposition at up to 3.2 m. The net landscape change during the modelled jökulhlaup was -86,400 m^3 (± 40 %), resulting from -275,400 m^3 (± 20 %) proglacial erosion and 194,400 m^3 (± 20 %) proglacial deposition. The rising limb pattern of bed elevation change suggested widespread activation of the bed, whereas the falling limb pattern suggested more organisation, perhaps primitive bedform development. Peak erosion rate and peak deposition rate were 650 m^3s^{-1} and 595 m^3s^{-1}, respectively, and coincided with peak discharge at 1.5 hours after flood initiation. Deposition occurred on the rising stage and erosion occurred on the falling limb, which is contrary to prevailing simple conceptual models.

Secondly, this study has several important implications for reconstructions of outburst floods at other sites. At its simplest, numerical modelling permits interpolation between (often sparse) field measurements. It permits discrimination of how an 'end-product' is obtained, in this case production of the post-flood landscape. However, analysing this spatiotemporal model output is challenging and needs development of automated grid-based programs (c.f. Carrivick et al., 2013a). Whether or not it is crucial to include sediment transport and morphodynamics in field (landscape) scale applications of numerical models of jökulhlaups or of other types of outburst floods depends on the intended application. This study has shown that inclusion of morphodynamics beyond a simpler hydrodynamic simulation accelerated the arrival time of the flow front and brought forwards the time of peak discharge. This is due to increased mass and momentum with sediment transport but also due to a feedback process whereby flow conveyance becomes more efficient due to (i) erosion of minor bed protrusions and (ii) deposition that infills or subdues minor bed hollows. Therefore hazard analyses focussed on inundation area need not go beyond hydrodynamic simulations, but those focussed on frontal wave arrival time and peak arrival time should note that the morphodynamic simulations of this study advanced those arrival timings by 100

% and 19 %, respectively. The peak magnitude of flow depth and flow velocity was not significantly affected by including morphodynamic processes.

Morphodynamic simulations can be extremely instructive for understanding rapid (minute-scale) landform construction and deposition process and products, but present challenges in parameterisation and validation. Most events will not have a pre-flood terrain model, especially at a high resolution, available and spatially distributed sediment characteristics can be hard to ascertain. This study found that over the course of the jökulhlaup, the pattern of erosion and deposition became more coherent, potentially indicative of bedform development. Total sediment transport became more ‘flashy’ over time, in contrast to discharge. Downstream variations in sediment transport, flow velocity, shear stress and flow discharge were largely a reflection of channel geometry: velocities and sediment transport were highest in constricted reaches and lower in unconfined reaches.

With regards to the opportunity presented by this modelling for process-product studies, future work should aim to target specific sediment-landform assemblages and examine energy exchanges between bed and flow, thereby beginning to bridge the gap in knowledge between grain-scale experiments and field-scale measurements. Refinements of the model presented here might include discrimination between vertical and lateral sediment via a slope failure operator for bank collapse, for example.

Acknowledgements

This research was funded by a NERC doctoral training grant awarded to KEHS at the University of Leeds. Matthew Roberts and Tomas Johannesson at the Icelandic Meteorological Office are thanked for their provision of data and advice, and Kristinn Sveinsson and Skúli Þorvaldsson at Loftmyndir ehf. and Bjarney Guðbjörnsdóttir and Dalia Prizginiene at Landmælingar Íslands are thanked for their provision of data and advice on data processing. Fiona Tweed, Andy Russell and Rob Duller discussed the 1999 event. Mingfu Guan, Andy Sleigh and Nigel Wright are thanked for their discussions on numerical modelling. Two anonymous reviewers, a special issue editor and Editor Stuart Lane are thanked for their scrutiny and constructive criticism.

References

Alho, P., and Aaltonen, J., 2008, Comparing a 1D hydraulic model with a 2D hydraulic model for the simulation of extreme glacial outburst floods: Hydrological Processes, v. 22, no. 10, p. 1537-1547.

Alho, P., Russell, A. J., Carrivick, J. L., and Kayhko, J., 2005, Reconstruction of the largest Holocene jökulhlaup within Jökulsá á Fjöllum, NE Iceland: Quaternary Science Reviews, v. 24, no. 22, p. 2319-2334.

Baker, V. R., 1996, Megafloods and glaciation., in Martini, I. P., ed., Late Glacial and Postglacial Environmental Changes: NY, Oxford University Press, p. 98-108.

Baker, V. R., 2002, High-energy megafloods: planetary setting and sedimentary dynamics, in Martini, I. P., Baker, V. R., and Garzon, G., eds., Flood and Megaflood Processes and Deposits: Recent and Ancient Examples.

Björnsson, H., 2009, Jökulhlaups in Iceland: sources, release and drainage, in Burr, D. M., Carling, P., and Baker, V. R., Eds., Megaflooding on Earth and Mars: Cambridge, Cambridge University Press, p. 50-64.

Begnudelli, L., and Sanders, B. F., 2007. Simulation of the St. Francis dam-break flood. Journal of Engineering Mechanics, v. 133, p. 1200-1212.

Bohorquez, P., and Darby, S. E., 2008. The use of one-and two-dimensional hydraulic modelling to reconstruct a glacial outburst flood in a steep Alpine valley. Journal of Hydrology, v. 361, p. 240-261.

Bridge, J. S., and Lunt, I. A., 2006, Depositional models of braided rivers, in Sambrook Smith, G. H., Best, J. L., Bristow, C. S., and Petts, G. E., eds., Braided Rivers: Special Publication Number 36 of the International Association of Sedimentologists. Malden, MA, Blackwell Publishing, p. 11-50.

Cao, Z., Pender, G., Wallis, S., Carling, P., 2004. Computational dam-break hydraulics over erodible sediment bed. Journal of Hydraulic Engineering-ASCE. v. 130, p. 689-703.

Capart, H., and Young, D.L., 1998. Formation of a jump by the dam-break wave over a granular bed. J Fluid Mech. v. 372, p. 165-87.

Carrivick, J. L., 2006, 2D modelling of high-magnitude outburst floods; an example from Kverkfjöll, Iceland. Journal of Hydrology, v. 321, p. 187-199.

Carrivick, J. L., 2007, Modelling coupled hydraulics and sediment transport of a high-magnitude flood and associated landscape change: Annals of Glaciology, v. 45, p. 143-154.

Carrivick, J. L., 2009, Jökulhlaups from Kverkfjöll volcano, Iceland: modelling transient hydraulic phenomena, in Burr, D. M., Carling, P., and Baker, V. R., eds., Megaflooding on Earth and Mars, Cambridge University Press. UK, pp. 273-289.

Carrivick, J. L., 2010, Dam break - Outburst flood propagation and transient hydraulics: Journal of Hydrology, v. 380, p. 338-355.

Carrivick, J.L., and Rushmer, E. L., 2006. Understanding high-magnitude outburst floods. Geology Today, v. 22, p. 60-65.

Carrivick, J.L., Russell, A.J., and Tweed, F.S., 2004a, Geomorphological evidence for jökulhlaups from Kverkfjöll volcano, Iceland. Geomorphology, v. 63, p. 81-102.

Carrivick, J.L., Russell, A.J., Tweed, F.S., and Twigg, D., 2004b, Palaeohydrology and sedimentology of jökulhlaups from Kverkfjöll, Iceland. Sedimentary Geology, v. 172, p. 19-40.

Carrivick, J. L., Manville, V., and Cronin, S. 2009, Modelling the March 2007 lahar from Mt Ruapehu. Bulletin of Volcanology, v. 71, p. 153-169.

Carrivick, J. L., Manville, V., Graettinger, A., and Cronin, S., 2010, Coupled fluid dynamics-sediment transport modelling of a Crater Lake break-out lahar: Mt. Ruapehu, New Zealand. Journal of Hydrology, v. 388, p. 399-413.

Carrivick, J. L., Jones, R., and Keevil, G., 2011, Experimental insights towards geomorphic processes within dam break outburst floods. Journal of Hydrology, v. 408, p. 153–163.

Carrivick, J. L., and Tweed, F. S., 2013, Proglacial lakes: character, behaviour and geological importance. Quaternary Science Reviews, v. 78, p. 34-52.

Carrivick, J. L., Turner, A. G. D., Russell, A. J., Ingeman-Nielsen, T., and Yde, J. C., 2013a, Outburst flood evolution at Russell Glacier, western Greenland: effects of a bedrock channel cascade with intermediary lakes. Quaternary Science Reviews, v. 67, p. 39–58.

Carrivick, J. L., Tweed, F. S., Carling, P., Alho, P., Marren, P. M., Staines, K., Russell, A. J., Rushmer, E. L., and Duller, R., 2013b, Discussion of ‘Field evidence and hydraulic modelling of a large Holocene jökulhlaup at Jökulsá á Fjöllum channel, Iceland’ by Douglas Howard, Sheryl Luzzadder-Beach and Timothy Beach, 2012. Geomorphology, 201, 512–519.

Cook, J. L., 1987, Quantifying peak discharges for historical floods: Journal of Hydrology, v. 96, no. 1-4, p. 29-40.

Costa, J. E., 1983, Palaeohydraulic reconstruction of flash-flood peaks from boulder deposits in the Colorado front range: Geological Society of America Bulletin, v. 94, p. 986-1004.

Costa, J. E., and Schuster, R. L., 1988, The formation and failure of natural dams: Geological Society of America Bulletin, v. 100, no. 7, p. 1054-1068.

Desloges, J. R., and Jones, D. P., 1989, Estimates of peak discharge from the drainage of ice-dammed Ape Lake, British Colombia, Canada: Journal of Glaciology, v. 35, no. 121, p. 349-354.

Emmett, M., and Moodie, T. B., 2008. Dam-break flows with resistance as agents of sediment transport. Physics of Fluids. 20, 086603.

Jónsdottir, K., Tryggvason, A., Roberts, R., Lund, B., Soosalu, H., and Bodvarsson, R., 2007, Habits of a glacier-covered volcano: seismicity patterns and velocity structure of Katla volcano, Iceland: Annals of Glaciology, v. 45, p. 169-177.

Scharrer, K., Spieler, O., Mayer, C., and Münzer, U., 2007, Imprints of sub-glacial volcanic activity on a glacier surface—SAR study of Katla volcano, Iceland: Bulletin of Volcanology, v. 70, no. 4, p. 495-506.

Fuamba, M., Bouaanani, N., and Marche, C., 2007, Modeling of dam break wave propagation in a partially ice-covered channel: Advances in Water Resources, v. 30, p. 2499-2510.

Fraccarollo, L., Capart, H., 2002. Riemann wave description of erosional dam-break flows. J Fluid Mech. 461, 183-228.

Guan, M., 2013. Geomorphic impacts of rapid sediment-laden flows through computational modelling. PhD thesis, University of Leeds. 177 pp.

Guan, M., Wright, N. G., and Sleigh, P. A., 2014. 2D process-based morphodynamic model for flooding by noncohesive dyke breach. Journal of Hydraulic Engineering, 140, 04014022.

Guan, M., Wright, N. G., and Sleigh, P. A., 2015. A multimode morphodynamic model for sediment-laden flows and geomorphic impacts. J. Hydraul. Eng., 10.1061/(ASCE)HY.1943-7900.0000997, 04015006.

Gudmundsson, M. T., Larsen, G., Hoskuldsson, A., and Gylfason, A. G., 2008, Volcanic hazards in Iceland: Jokull, v. 58, p. 251-268.

Herget, J., 2005. Reconstruction of Pleistocene ice-dammed lake outburst floods in the Altai Mountains, Siberia Geological Society of America Special Publications, v. 386.

Huang, W., Cao, Z. X., Carling, P., and Pender, G., 2014, Coupled 2D hydrodynamic and sediment transport modeling of megaflood due to glacier dam-break in Altai Mountains, Southern Siberia. Journal of Mountain Science, v. 11, p. 1442-1453.

Jaenicke, J., Mayer, C., Scharrer, K., Muenzer, U., and Gudmundsson, A., 2006, The use of remote-sensing data for mass-balance studies at Myrdalsjokull ice cap, Iceland: Journal of Glaciology, v. 52, no. 179, p. 565-573.

Jarrett, R. D., 1987, Errors in slope-area computation of peak discharges in mountain stream: Journal of Hydrology, v. 96, no. 1-4, p. 53-67.

Kamrath, P., Disse, M., Hammer, M., and Kongeter, J., 2006, Assessment of discharge through a dike breach and simulation of flood wave propagation: Natural Hazards, v. 38, no. 1-2, p. 63-78.

Koike, T., and Takenaka, S., 2012. Scenario analysis on risks of glacial lake outburst floods on the Mangde Chhu River, Bhutan. Global Environmental Research, 16, 41-49.

Lane, S.N., Westaway, R.M., Hicks, D.M., 2003. Estimation of erosion and deposition volumes in a large, gravel-bed, braided river using synoptic remote sensing. Earth Surface Processes and Landforms, v. 28, p. 249-271.

Lawler, D. M., 1994, Recent changes in rates of suspended sediment transport in the Jökulsá á Sólheimasandi glacial river, southern Iceland: Variability in Stream Erosion and Sediment Transport, p. 343-350.

Lawler, D. M., and Brown, R. M., 1992, A simple and inexpensive turbidity meter for the estimation of suspended sediment concentrations: Hydrological Processes, v. 6, no. 2, p. 159-168.

Lesser, G. R., Roelvink, J. A. van Kester, J. A. T. M. and Stelling G. S., 2004. Development and validation of a three-dimensional morphological model. Coastal Engineering, v. 51, p. 883-91.

Lube, G., Cronin, S. J., Manville, V., Procter, J. N., Cole, S. E., and Freundt, A., 2012. Energy growth in laharic mass flows. Geology, v. 40(5), p. 475-478.

Magilligan, F. J., Gomez, B., Mertes, L. A. K., Smith, L. C., Smith, N. D., Finnegan, D., and Garvin, J. B., 2002. Geomorphic effectiveness, sandur development, and the pattern of landscape response during jökulhlaups: Skeiðarársandur, southeastern Iceland. Geomorphology, 44(1), p. 95-113.

Maizels, J., 1989a, Sedimentology and palaeohydrology of Holocene flood deposits in front of a jokulhlaup glacier, south Iceland, in Bevan, K., and Carling, P. A., eds., Floods: Hydrological, Sedimentological and Geomorphological Implications: Chichester, John Wiley and Sons, p. 239-251.

Maizels, J., 1989b, Sedimentology, paleoflow dynamics and flood history of jökulhlaup deposits - paleohydrology of Holocene sediment sequences in southern Iceland sandur deposits: Journal of Sedimentary Petrology, v. 59, no. 2, p. 204-223.

Maizels, J., 1991, The origin and evolution of Holocene sandur deposits in areas of jokulhlaup drainage, Iceland, in Maizels, J., and Caseldine, C., eds., Environmental Change in Iceland: Past and Present: Netherlands, Kluwer Academic Publishers, p. 267-302.

Maizels, J., 1992, Boulder ring structures produced during jökulhlaup flows: Geografiska Annaler. Series A, Physical Geography, v. 74, no. 1, p. 21-33.

McGuire, B., 2013. Hazardous responses of the solid Earth to a changing climate. Climate Forcing of Geological Hazards, 1-33.

Mountney, N. P., and Russell, A. J., 2006, Coastal aeolian dune development, Solheimasandur, southern Iceland: Sedimentary Geology, v. 192, no. 3-4, p. 167-181.

Pagli, C., and Sigmundsson, F., 2008, Will present day glacier retreat increase volcanic activity? Stress induced by recent glacier retreat and its effect on magmatism at the Vatnajökull ice cap, Iceland: Geophysical Research Letters, v. 35, p. 1-5.

Pitman, E. B., Patra, A. K., Kumar, D., Nishimura, K., and Komori, J., 2013. Two phase simulations of glacier lake outburst flows. Journal of Computational Science, v. 4, no. 1, 71-79.

Pritchard, D., and Hogg, A.J., 2002. On sediment transport under dam-break flow. J Fluid Mech., 473, 265-74.

Richardson, S. D., and Reynolds, J. M., 2000, An overview of glacial hazards in the Himalayas: Quaternary International, v. 65-6, p. 31-47.

Rijn, L.C. van, 1993. Principles of Sediment Transport in Rivers, Estuaries and Coastal Seas. Aqua Publications, The Netherlands.

Roberts, M. J., Tweed, F. S., Russell, A. J., Knudsen, O., and Harris, T. D., 2003, Hydrologic and geomorphological effects of temporary ice-dammed lake formation during jokulhlaups: Earth Surface Processes and Landforms, v. 28, no. 7, p. 723-737.

Rushmer, E. L., 2007 Physical-scale modelling of jökulhlaups (glacial outburst floods) with contrasting hydrograph shapes: Earth Surface Processes and Landforms, v. 32, no. 6, p. 954-963.

Rushmer, E. L., Russell, A. J., Tweed, F. S., Knudsen, O., and Marren, P. M., 2002, The role of hydrograph shape in controlling glacier outburst flood (jokulhlaup) sedimentation, in Dyer, F. J. T. M. C. O. J. M., ed., Structure, Function and Management Implications of Fluvial Sedimentary Systems, p. 305-313.

Russell, A. J., Tweed, F. S., Knudsen, O., Roberts, M. J., Harris, T. D., and Marren, P. M., 2002a, Impact of the July 1999 jokulhlaup on the proximal river jokulsa a solheimasandi, myrdalsjokull glacier, southern Iceland, Extremes of the Extremes: Extraordinary Floods, p. 249-254.

Russell, A. J., Tweed, F. S., Knudsen, O., Roberts, M. J., Harris, T. D., and Marren, P. M., 2002b, The geomorphological impact and sedimentary characteristics of the July 1999 jökulhlaup on the Jökulsá á Sólheimasandi, Mýrdalsjökull, southern Iceland., in Snorrason, A. F. H. P. M. M. E., ed., Extremes of the Extremes: Extraordinary Floods, p. 249-254.

Russell, A. J., Roberts, M. J., Fay, H., Marren, P. M., Cassidy, N. J., Tweed, F. S., and Harris, T., 2006, Icelandic jökulhlaup impacts: Implications for ice-sheet hydrology, sediment transfer and geomorphology: Geomorphology, v. 75, no. 1-2, p. 33-64.

Russell, A. J., Tweed, F. S., and Knudsen, Ó., 2000, Flash flood at Sölheimajökull heralds the reawakening of an Icelandic subglacial volcano: Geology Today, v. 16, no. 3, p. 102-106.

Russell, A. J., Tweed, F. S., Roberts, M. J., Harris, T. D., Guðmundsson, M. T., Knudsen, Ó., and Marren, P. M., 2010, An unusual jökulhlaup resulting from subglacial volcanism, Sólheimajökull, Iceland: Quaternary Science Reviews, v. 29, no. 11-12, p. 1363-1381.

Smith, K. T., and Dugmore, A. J., 2006, Jökulhlaups circa Landnám: mid- to late first millennium AD floods in south Iceland and their implications for landscapes of settlement: Geografiska Annaler, v. 88A, no. 2, p. 165-176.

Smith, L. C., Sheng, Y., Magilligan, F.J., Smith, N.D., Gomez, B., Mertes, L.A.K., Krabill, W.B., and Garvin, J.B., 2006. Geomorphic impact and rapid subsequent recovery from the 1996 Skeiðarársandur jökulhlaup, Iceland, measured with multi-year airborne lidar. Geomorphology, v. 75, p. 65-75.

Sigurðsson, O., Zóphóníasson, S., and Ísleifsson, E., 2000, Jökulhlaup úr Sólheimajökull 18, júlí 1999: Jökull, v. 49, p. 75-81.

Staines, K. E., Carrivick, J. L., Tweed, F. S., Evans, A. J., Russell, A. J., Jóhannesson, T., and Roberts, M., 2014. A multi-dimensional analysis of proglacial landscape change at Sólheimajökull, southern Iceland. Earth Surface Processes and Landforms. Available online from 14/11/2014.

Swartenbroekx, C., Zech, Y., and Soares-Frazão, S., 2013. Two-dimensional two-layer shallow water model for dam break flows with significant bed load transport. International Journal for Numerical Methods in Fluids, v. 73, 477-508.

Tweed, F. S., 1998, An ice-dammed lake in Jökulsárgil: predictive modelling and geomorphological evidence: Jökull, v. 48, p. 17-28.

Williams, R. D., Brasington, J., Hicks, M., Measures, R., Rennie, C. D., and Vericat, D., 2013. Hydraulic validation of two-dimensional simulations of braided river flow with spatially continuous ADCP data. Water Resources Research, v. 49, 5183-5205.

Worni, R., Stoffel, M., Huggel, C., Volz, C., Casteller, A., and Luckman, B., 2012. Analysis and dynamic modeling of a moraine failure and glacier lake outburst flood at Ventisquero Negro, Patagonian Andes (Argentina). Journal of Hydrology, 444, 134-145.

Wu, W.M., and Wang, S.S.Y., 2007. One-dimensional Modeling of dam-break flow over movable beds. Journal of Hydraulic Engineering-ASCE. 133, 48-58.

Xia, J., Lin, B., Falconer, R. A., and Wang, G., 2010. Modelling dam-break flows over mobile beds using a 2D coupled approach. Advances in Water Resources. 33, 171-83.

Zech, Y., Soares-Frazao, S., Spinewine, B., and Grelle N. L., 2008. Dam-break induced sediment movement: Experimental approaches and numerical modelling. Journal of Hydraulic Research. V. 46, 176-90.

Geomorphological impact and morphodynamic effects on flow conveyance of the 1999 jökulhlaup at Sólheimajökull, Iceland

Kate E. H. Staines and Jonathan L. Carrivick

Hydrodynamic reconstructions of field (landscape) scale outburst floods
1D Magilligan et al., (2002), Skeiðarársandur, Iceland. Alho *et al*., (2005), Jökulsá á Fjöllum, Iceland. Herget (2005), Altai floods, Siberia, Russia.
1D-2D Kamrath *et al*. (2006), dike breach on River Rhine.
2D Begnudelli and Sanders (2007), St Francis, California. Fuamba *et al*. (2007), Quebec. Carrivick, (2006, 2007); Kverkfjöll, Iceland. Carrivick *et al*. (2009, 2011*), Ruapehu, NZ. Carrivick *et al*. (2013a); Russell Glacier, w. Greenland. Bohorquez and Darby (2008). Mont Miné, Switz. Miyamoto *et al*. (2006, 2007), Denlinger and O'Connell, (2010), Alho *et al*. (2010); Missoula flooding, NW USA. Carling *et al*. (2010), Altai floods, Siberia, Russia. Worni *et al*. (2012)*, Ventisquero Negro, Patagonia. Koike and Takenaka (2012), Mangde Chhu, Bhutan. Pitman *et al*. (2013), Lugge Lake, Bhutan. Westoby *et al*. (2014), Chukhung Glacier, Nepal.

Table 1. Selected examples of application of numerical models of outburst floods, mostly to jökulhlaups, at the field (landscape) scale, for both palaeo and modern studies. *Only the models applied by Carrivick *et al*. (2011), Worni *et al*. (2012) and Pitman *et al*. (2013) include sediment transport.

Geomorphological impact and morphodynamic effects on flow conveyance of the 1999 jökulhlaup at Sólheimajökull, Iceland

Kate E. H. Staines and Jonathan L. Carrivick

Axis Length (mm)			Velocity (v)	Shear Stress (τ)	Stream Power (ω)	Flow Depth (D)
a	b	c	m s^{-1}	N m^{-2}	W m^{-2}	m
10750	8410	3720	15	3,200	37,200	9.7
10250	6370	750	13	2,300	23,300	7.9
9900	5900	4400	12	2,100	20,500	7.5
8450	6180	5070	13	2,200	22,200	7.7
8200	3550	2270	10	1,100	8,700	5.2
	Mean		13	2,200	21,600	7.6

Table 2: Palaeocompetence reconstructions using the five largest clasts of 395 boulders measured on the boulder fan and via the equations of Costa (1983).

Geomorphological impact and morphodynamic effects on flow conveyance of the 1999 jökulhlaup at Sólheimajökull, Iceland

Kate E. H. Staines and Jonathan L. Carrivick

Palaeohydraulic Method	Velocity ($m.s^{-1}$)	Shear Stress ($N\ m^{-2}$)	Stream Power (ω)	Flow Depth (m)
Palaeocompetence (point) measurements	13 (mean)	2200	21,600	7.6
Slope-area reconstructions (Russell *et al.* 2010)	~5 – 7	930 to 1,280	~5,200 to 8,200	3.3 to 4.8
Hydrodynamic modelling	0.9 (average) 8.6 (max)	110 (average) 3,430 (max)	n/a	12 (cross-section 1)

Table 3: Comparison of palaeohydraulic reconstructions at the glacier terminus

Geomorphological impact and morphodynamic effects on flow conveyance of the 1999 jökulhlaup at Sólheimajökull, Iceland

Kate E. H. Staines and Jonathan L. Carrivick

Parameter	Hydrodynamic	Morphodynamic simulation
	For whole model domain	
Mean front velocity ($m.s^{-1}$)	1.06	2.14
Inundation area (m^2)	3,668,490	3,681,220
Sediment moved (m^3)	-	469,800
	By way of example, for cross-section 7, 7.05 km from ice margin	
Flow depth max. (m)	3.75	3.4
Time of peak flow	01:20 after start	01:05 after start
Cumulative bed elevation change (m)	-	0.88
Time of max. bed level	-	06:15
Velocity max. ($m.s^{-1}$)	3.95	4.21
Max. bedload transport rate: all fractions ($m^3.s^{-1}.m^{-1}$)	-	0.0116
Max. bed shear stress ($N.m^{-2}$)	-	308.75

Table 4. Summary of results of hydrodynamic and morphoynamic simulations

Geomorphological impact and morphodynamic effects on flow conveyance of the 1999 jökulhlaup at Sólheimajökull, Iceland

Kate E. H. Staines and Jonathan L. Carrivick

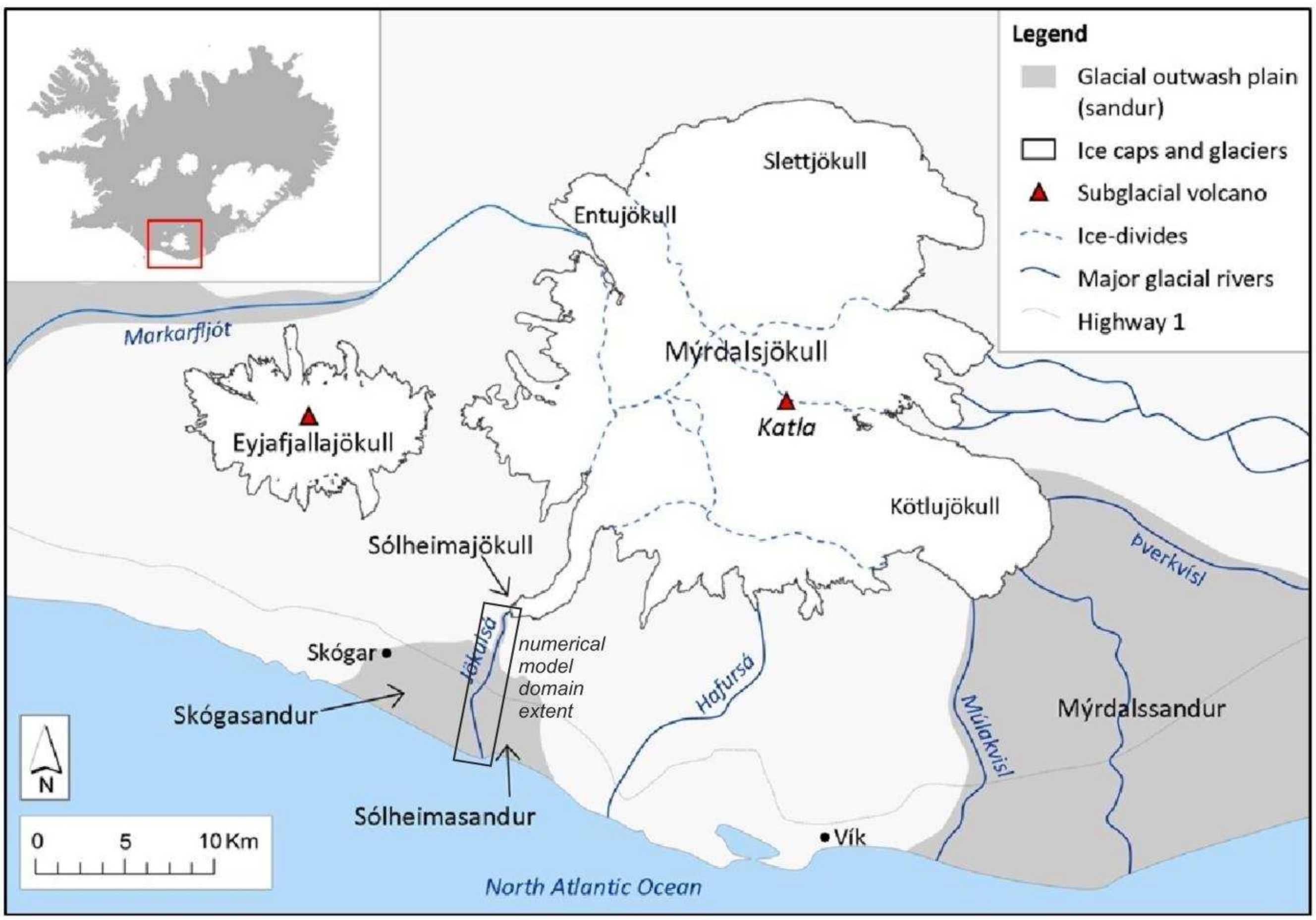

Figure 1: Location of Solheimajokul and Solheimasandur on the southern margin of Myrdalsjokull in southern Iceland. The numerical model domain used in this study is indicated.

Geomorphological impact and morphodynamic effects on flow conveyance of the 1999 jökulhlaup at Sólheimajökull, Iceland

Kate E. H. Staines and Jonathan L. Carrivick

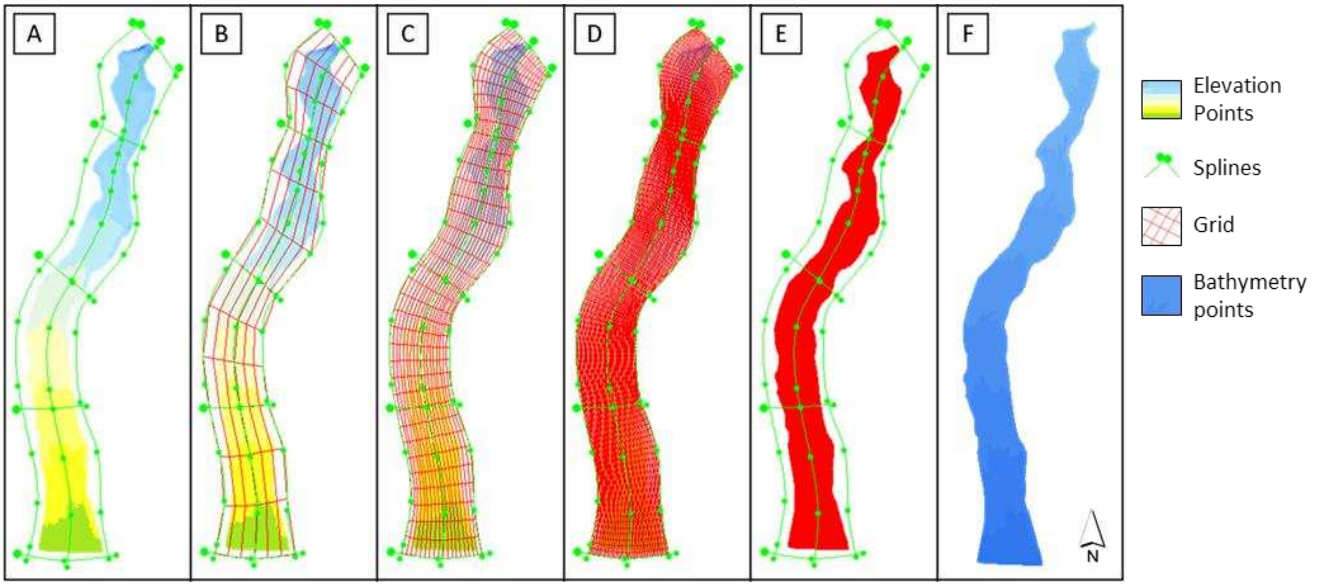

Figure 2: Steps involved in the creation of the curvilinear grid. [A] Splines are defined using sample points as a guide; [B] Splines interpolated to grid; [C] Grid refined; [D] Grid refined and orthogonalised; [E] Grid clipped to desired extent of model; [F] Bathymetry points mapped onto mesh.

Geomorphological impact and morphodynamic effects on flow conveyance of the 1999 jökulhlaup at Sólheimajökull, Iceland

Kate E. H. Staines and Jonathan L. Carrivick

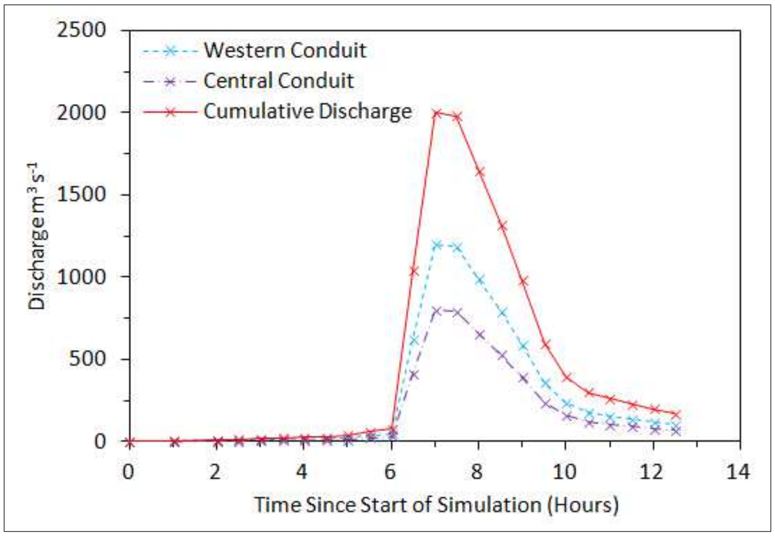

Figure 3: Input hydrograph to Delft3d as defined by: field measurements of river stage and discharge of 1700 m^3s^{-1} made at the bridge by Sigurðsson et al. (2000); the peak discharge estimates of Russell et al. (2010); and knowledge of the flood trigger. The first 6 hours of the hydrograph are the input values for the ‘baseflow model’ and the following 6 ½ hours are the ‘jökulhlaup model’.

Geomorphological impact and morphodynamic effects on flow conveyance of the 1999 jökulhlaup at Sólheimajökull, Iceland

Kate E. H. Staines and Jonathan L. Carrivick

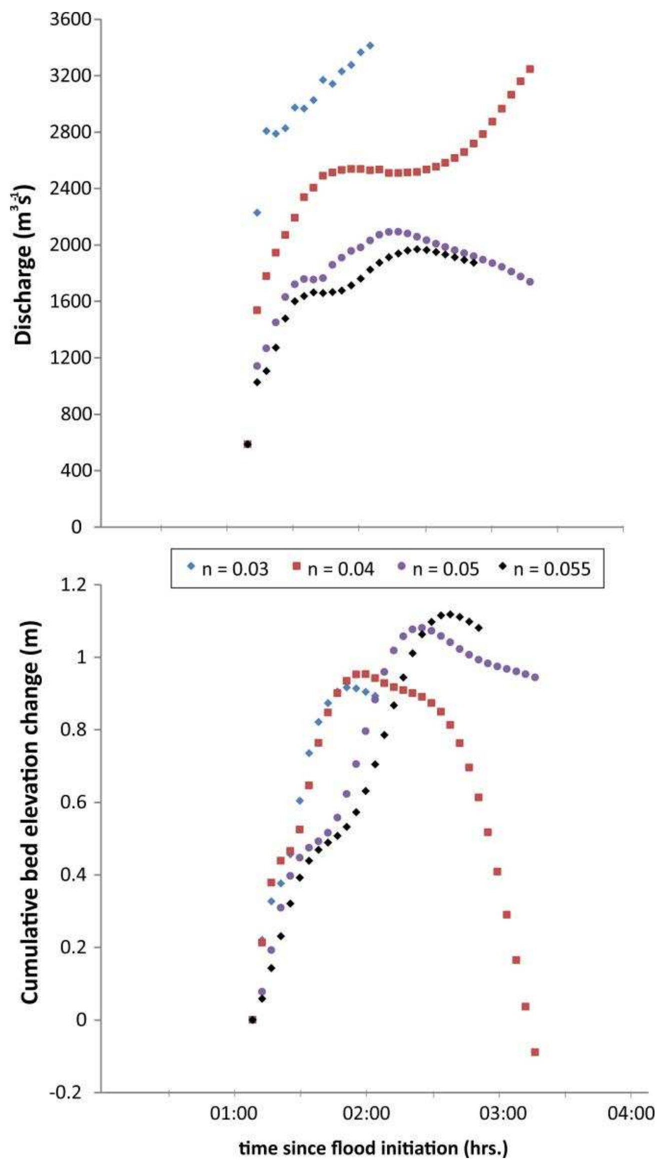

Figure 4. Sensitivity of cross-sectional discharge and mean cross-sectional bed elevation change to Manning's n roughness. Cross-section is 50 m upstream from the downstream boundary.

Geomorphological impact and morphodynamic effects on flow conveyance of the 1999 jökulhlaup at Sólheimajökull, Iceland

Kate E. H. Staines and Jonathan L. Carrivick

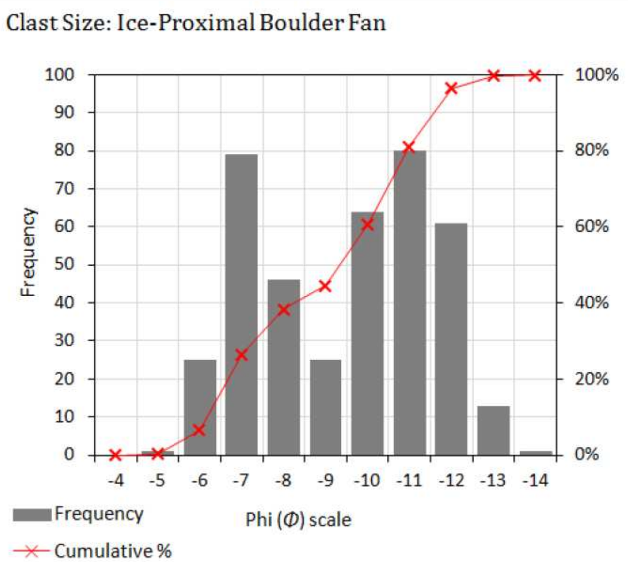

Φ scale	Size Range (mm)	Wentworth Size Class
-14	16384 to 8192	Very Large Boulder
-13	8192 to 4096	
-12	4096 to 2048	
-11	2048 to 1024	Large Boulder
-10	1024 to 512	Medium Boulder
-9	512 to 256	Small Boulder
-8	256 to 128	Large Cobble
-7	128 to 64	Small Cobble
-6	64 to 32	Very coarse gravel
-5	32 to 16	Coarse gravel
-4	16 to 8	Medium gravel

Total clast count = 395

Figure 5. Clast size analysis of the ice-proximal boulder fan.

Geomorphological impact and morphodynamic effects on flow conveyance of the 1999 jökulhlaup at Sólheimajökull, Iceland

Kate E. H. Staines and Jonathan L. Carrivick

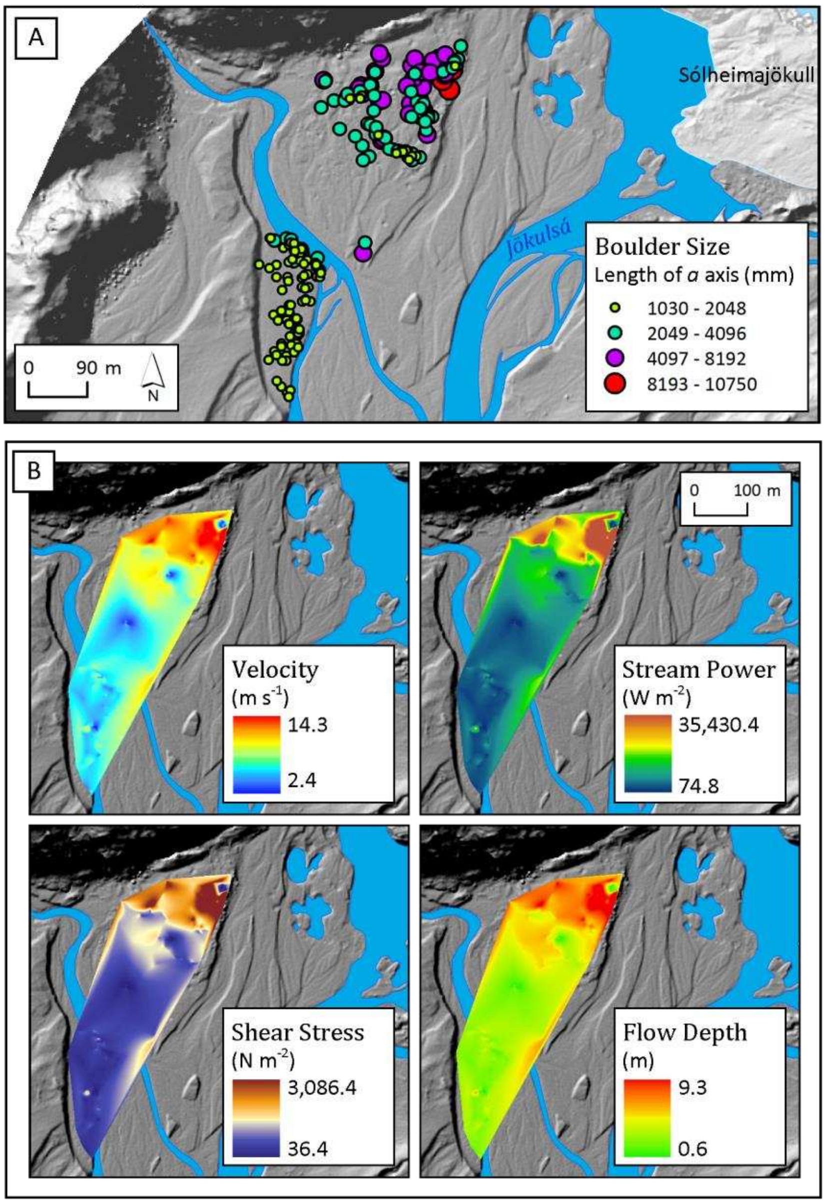

Figure 6: [A] Size of clasts measured at the ice-proximal boulder fan. [B] Flow parameters reconstructed using the palaeocompetence technique. Note that there are some minor interpolation effects along the periphery of each map in B.

Geomorphological impact and morphodynamic effects on flow conveyance of the 1999 jökulhlaup at Sólheimajökull, Iceland

Kate E. H. Staines and Jonathan L. Carrivick

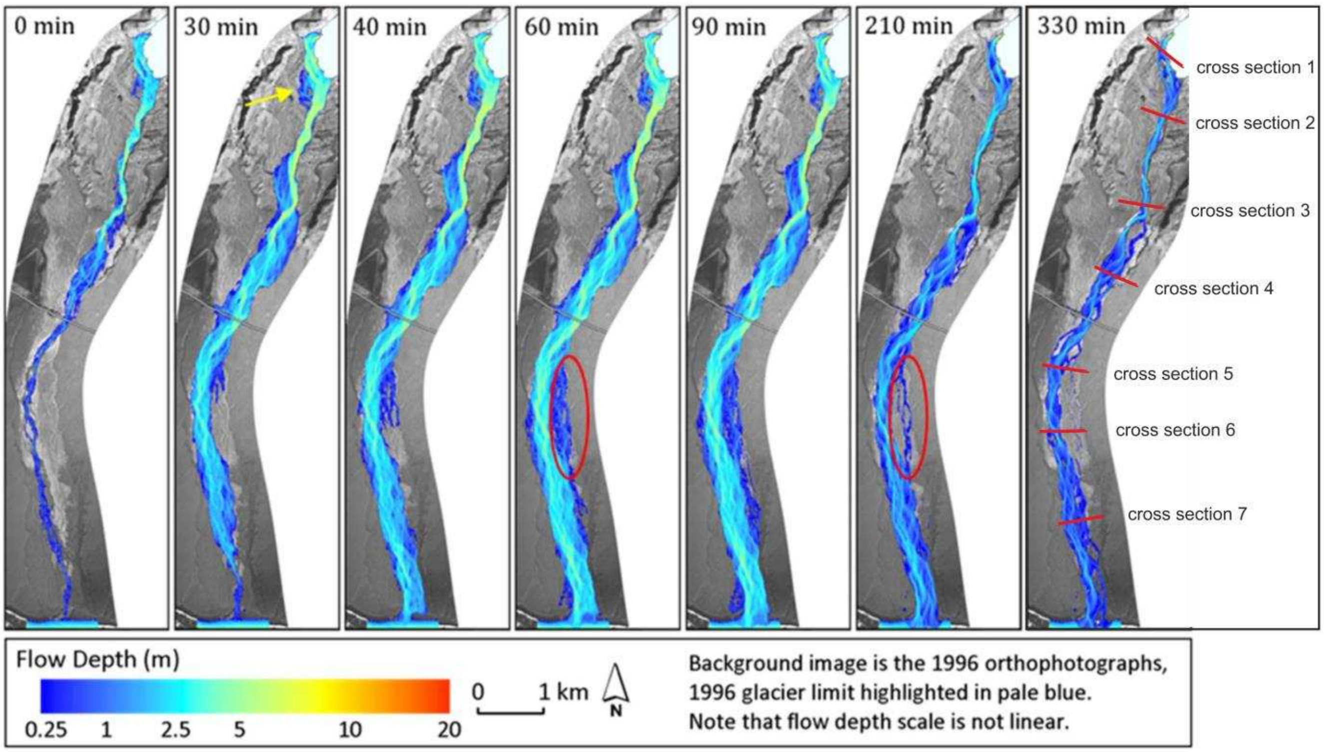

Figure 7: Modelled flow depth for duration of simulated jökulhlaup. Note the wetting and drying effect at the edges of the flood, highlighted in red. Yellow arrow highlights area of palaeo-channel reactivation near the ice-margin. Time in minutes since flood initiation are shown in the top left corner of each image.

Geomorphological impact and morphodynamic effects on flow conveyance of the 1999 jökulhlaup at Sólheimajökull, Iceland

Kate E. H. Staines and Jonathan L. Carrivick

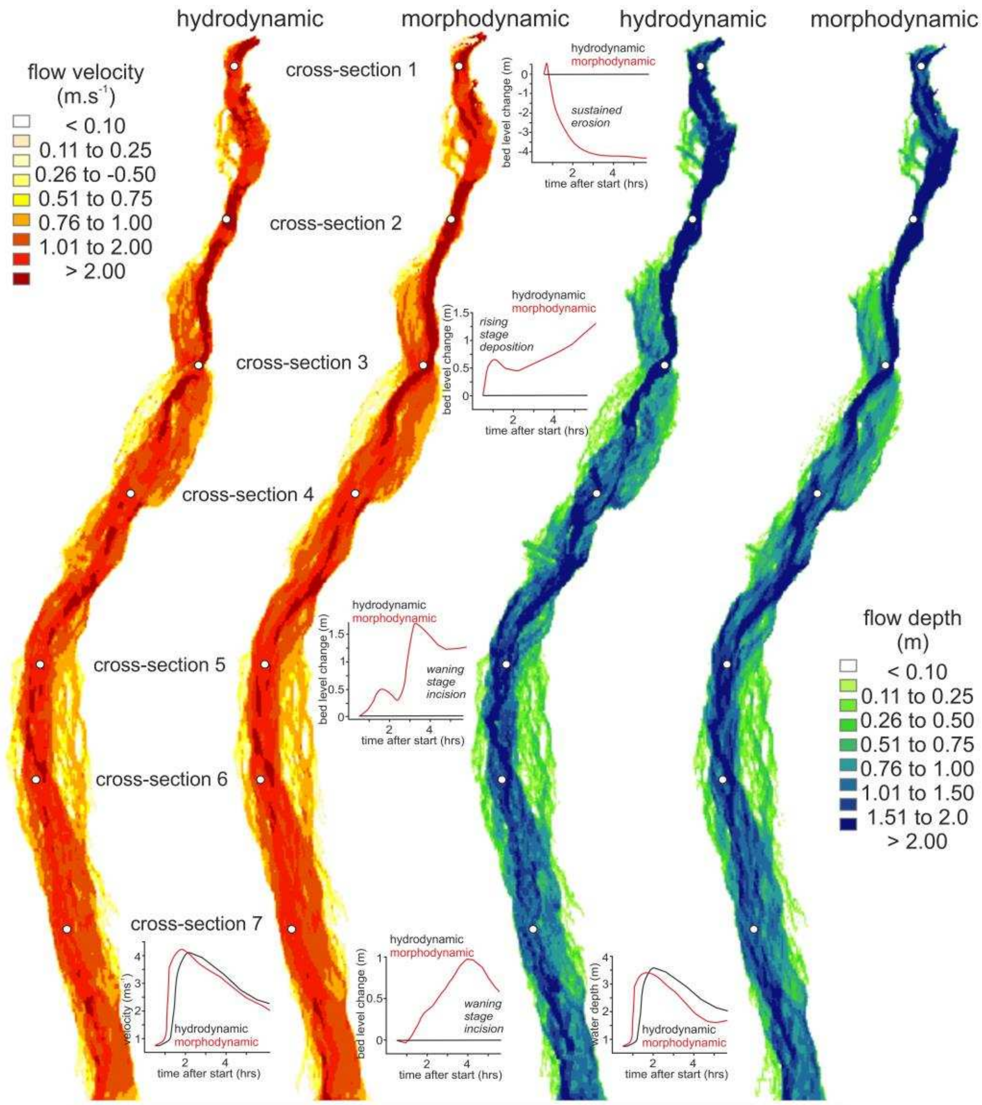

Figure 8. Comparison of spatiotemporal hydrodynamic and morphodynamic simulations. Maps pertain to time 01:30 after flood initation. Note that deeper and faster flow occurred than legend suggests, but colour scale is optimised to show variability. Note only bed elevation is plotted for cross-sections 1, 3, 5 and 7, and flow velocity and flow depth are only plotted for cross-section 7, for brevity and clarity. Note changing y-scale for bed elevation. More temporal information on hydraulics at each cross-section is given in Figure 7 and for cross-sections in Figure 9.

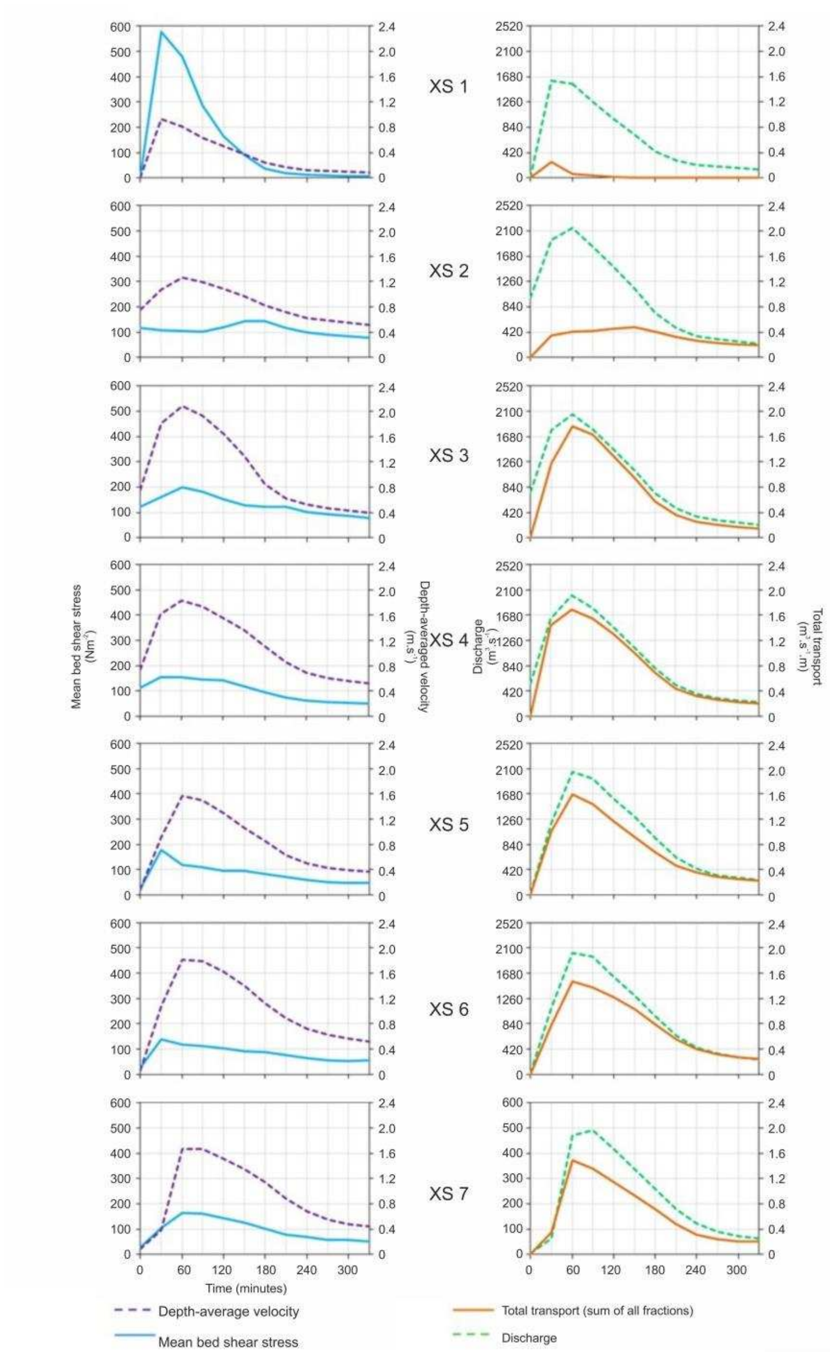

Figure 9: Downstream variation in modelled hydraulic parameters for the morphodynamic model run.

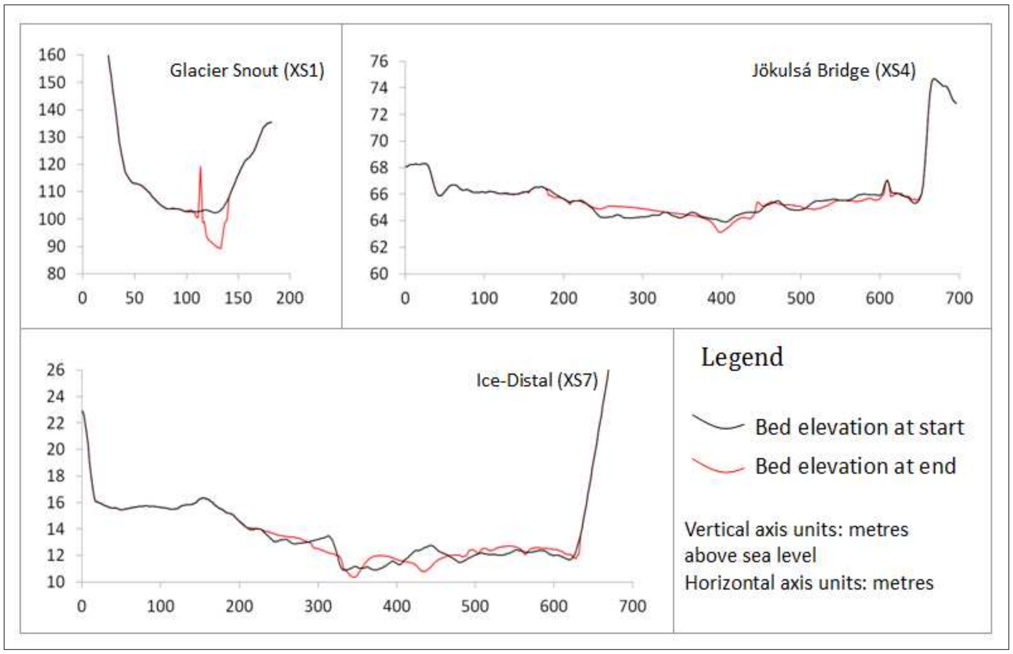

Figure 10: Bed elevations at three cross-sections at the start of the modelled jökulhlaup (0 minutes) and at the end (330 minutes). The spike in elevation gained at cross-section 1 remains unexplained. Cross-sectional distance x-axis is measured from the true left bank. For location of cross-sections, see Figure 8.

Geomorphological impact and morphodynamic effects on flow conveyance of the 1999 jökulhlaup at Sólheimajökull, Iceland

Kate E. H. Staines and Jonathan L. Carrivick

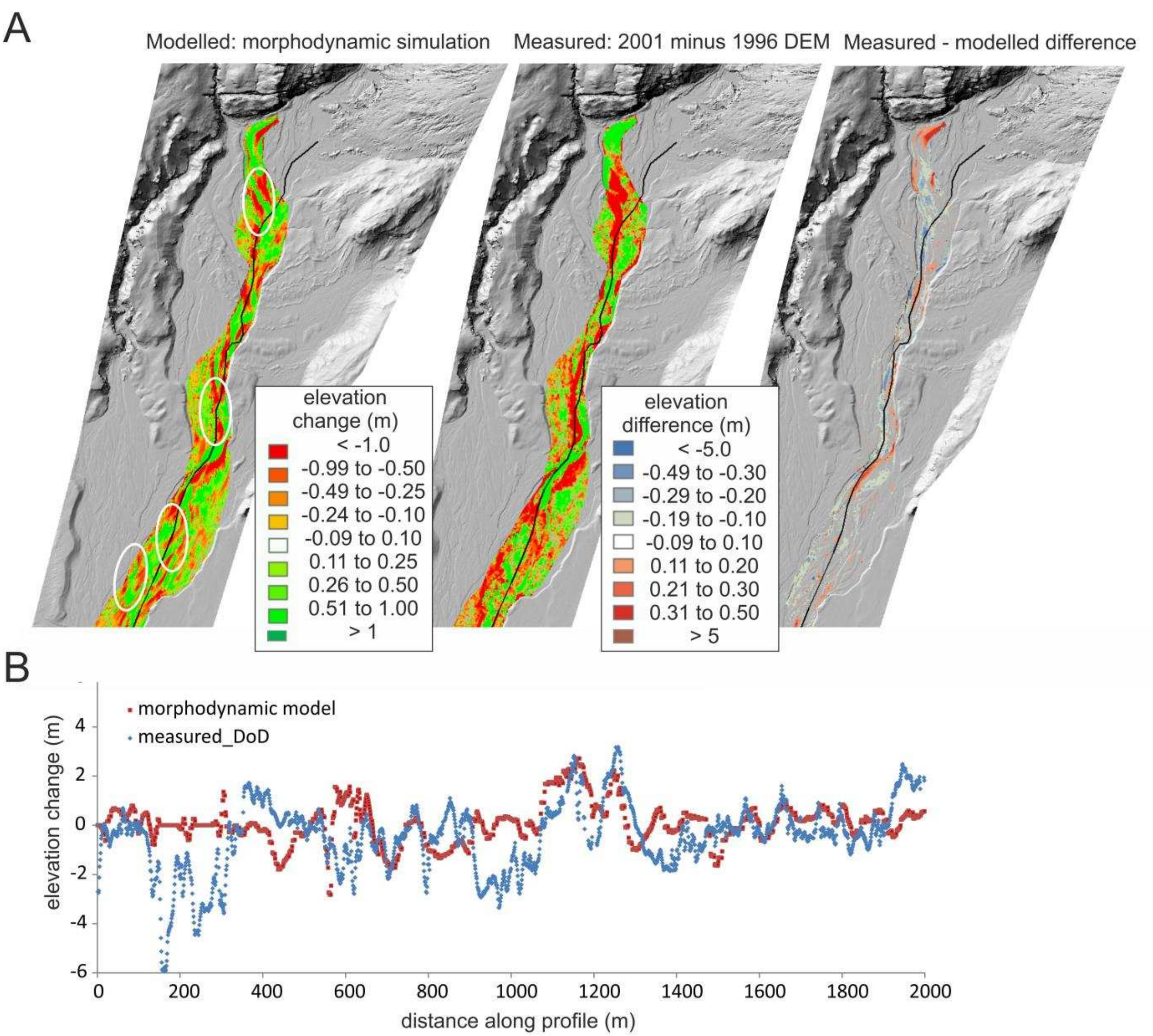

Figure 11. Comparison of DEM of difference between 1996 and 2001, and the net cumulative elevation changes as a result of the morphodynamic model, in part [A] both overlayed on the 2010 LiDAR-derived hillshaded DEM. Note colour scale in part A is to emphasise detail and values < -1.0 and > 0.5 did occur. Black line in part [A] is the long profile along which elevation differences are plotted in part [B]. White ellipses in A delimit zones mentioned in the text.

Geomorphological impact and morphodynamic effects on flow conveyance of the 1999 jökulhlaup at Sólheimajökull, Iceland

Kate E. H. Staines and Jonathan L. Carrivick

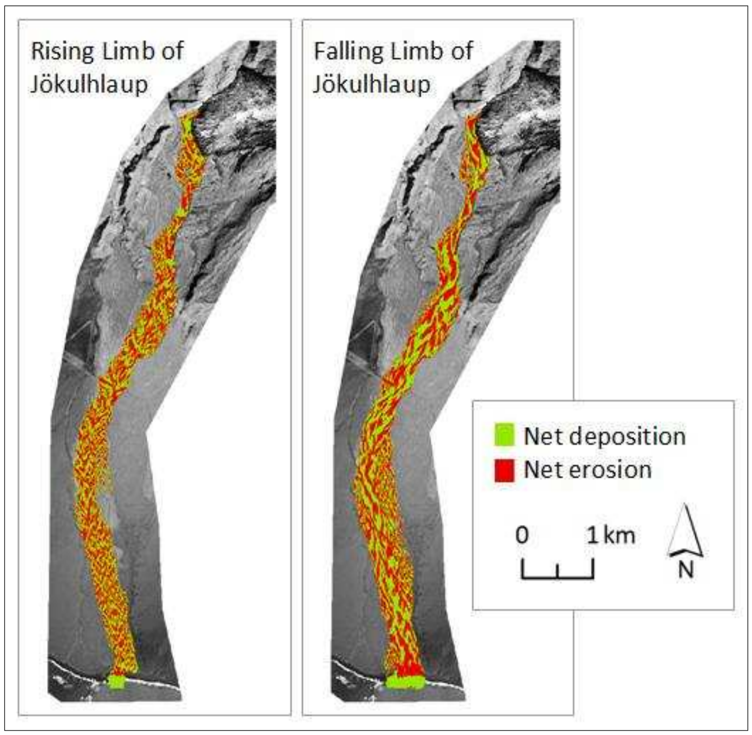

Figure 12. Pattern of cumulative bed elevation change discriminated by rising and falling hydrograph limbs, overlayed on aerial photograph mosaic.

Geomorphological impact and morphodynamic effects on flow conveyance of the 1999 jökulhlaup at Sólheimajökull, Iceland

Kate E. H. Staines and Jonathan L. Carrivick

Supplementary material: video (.avi) files of spatiotemporal flow depth, velocity, bed shear stress, froude number, total sediment transport and cumulative bed elevation change.